Tutors

Dra. Alexandra E. Bonet Ruiz

Dr. Ricardo Torres Castillo

Secció Departamental
d'Enginyeria Química

Màster en Enginyeria Química

CFD modelling with MFIX® of liquid-solid fluidized beds of polydisperse struvite crystals

Modelització per CFD amb MFIX® de llits fluïditzats líquid-sòlid de cristalls de struvita polidispersos

Ricardo Moya Chamizo

June, 2019

Treball Final de Màster

UNIVERSITAT DE BARCELONA

Dos campus d'excel·lència internacional

B:KC Barcelona Knowledge Campus

HUBC Health Universitat de Barcelona Campus

Aquesta obra està subjecta a la llicència de:

Reconeixement–NoComercial-SenseObraDerivada

http://creativecommons.org/licenses/by-nc-nd/3.0/es/

En primer lloc, agrair als meus pares als antics companys de classe i als actuals companys de treball tota la confiança, ànims i suport absoluts que m'han prestat, sense ells tot hauria sigut molt complex.

En segon lloc, dono les gracies als meus tutors, Ricard Torres i Alexandra Bonet, per les ajudes indiscutibles rebudes per part seva, tant referides al treball com consells aleatoris de tots els camps d'enginyeria, i sobretot pel seu comportament humà.

Finalment dono les gracies a la resta del professorat, per tot el que he après gracies a les seves classes i per conseqüència la confiança personal que he guanyat en vers a la vida laboral.

REPORT

CONTENTS

1. SUMMARY

This final master project aims to model with computational fluid dynamics a fluidized bed of polydisperse struvite crystals to analyze, study and compare the fluid dynamic properties of the bed against the results that (Md. Saifur, et al. 2017) show in their article (CFD modeling of liquid-solid fluidized beds of polydisperse struvite crystals) published the 21 October of 2017.

A steady state is reached through a transient study of polydisperse solids initially packaged. These solids are fluidized at different up-flow velocities (different case studies). The validation is going to be done once the steady state is reached at the real time of 120 s. Also, the characteristic fluidization heights reached in the steady state are evaluated for each set of solids of a determined diameter. The validation data between the simulation and the pilot plant (literature) is the time averaged liquid volume fraction (also known as bed voidage and being the complementary value to the solids fraction).

Each MFIX® used module is described. The explained modules are the geometry design, FAVOR (fractional area/volume orthogonal) mesh generation, region generation and the boundary and initial conditions.

ParaView® open code program is used to analyze, interpret and study the exported results. The data is shown in vector and contour picture scale and in numerical-graphical level for each exported time step data. Also, videos that reproduce the virtual reality of the study are exported from ParaView®.

The chosen geometry has been 2D, in order to reduce the computational time and to adapt better the FAVOR mesh to the studied region.

The bed dimension is a cylinder with 1392 mm high and 100 mm diameter. The pilot plant was done in a 20 ºC temperature-controlled room, thereby this value is constant in all the studies. The system outlet pressure is 1 atm (boundary condition for all case studies). The bed inlet velocity is a uniform inlet up-flow velocity, the value of this boundary condition is changed for all different case studies.

The values predicted by both ANSYS® and MFiX® CFD simulated models are in excellent agreement with the pilot plant experimental data obtained by (Md. Saifur, et al. 2017).

2. INTRODUCTION

One of the processes in which more amount of orthophosphate is released is in the secondary anaerobic digestion (SAD) phase of the biological nutrient removal (BNR). See Figure 1. As it is one of the most common water treatment processes applied at industrial level, is important to note that any benefit that can be given to this orthophosphate obtained by these processes, will be a breakthrough for the treatment of "waste".

Under favorable conditions, this high level of phosphates in anaerobic digester supernatant can cause struvite ($MgNH_4PO_4 \cdot 6H_2O$) precipitation in the digester line.

Struvite, also referred to as MAP, forms when there is a mole to mole to mole ratio (1:1:1) of magnesium, ammonia and phosphate in the wastewater.

With those elements in place, struvite is more likely to form in a high pH environment, where there is higher conductivity, lower temperatures, and higher concentrations of magnesium, ammonia and phosphate.

Having struvite scale in a wastewater treatment system can lead to great inefficiency within the plant or operation due to clogging of the pipes, pumps and equipment. There have been a few options to solve this issue, including replacing the pipes, or using a hydro-jetter or a mechanical grinder to clear them. But many lines can be underground and either of these options implies considerable downtime and labor.

As said above, this precipitated struvite can produce catastrophic effects in pipeline networks (see Figure 2). As well as producing unwanted effects in valves, pumps, heat exchangers etc. It is known that by the shape of these struvite crystals (see Figure 3), their ease of aligning in the direction of the flow causes them to travel throughout the installation. This makes it possible to produce problems anywhere. And if the sustainable flow of the installation is not enough, they could even accumulate and produce plugs that generate undesired back pressure and critical effects in the installation. (Mavinic, et al. 2007)

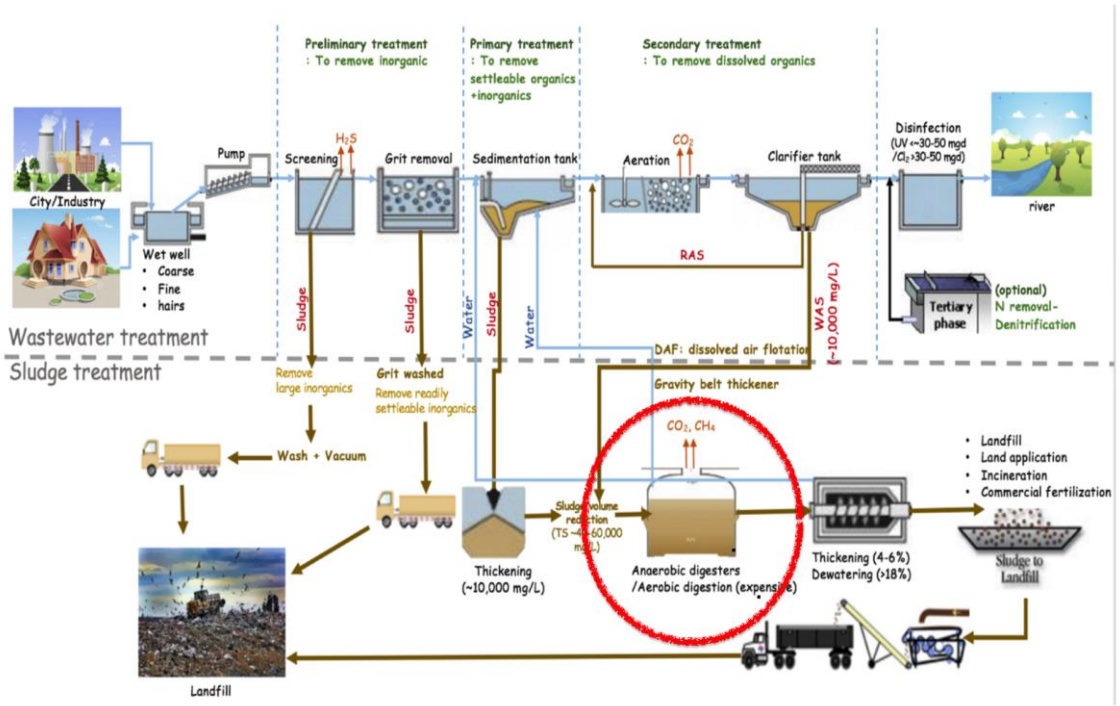

Figure 1. Wastewater Treatment Process Diagram (in the red circle there is the SAD)

Figure 2. Wastewater Treatment Struvite Plugged pipeline. (CED)

The most typical places where these crystals precipitate are (see Figure 3) elbows and pump suction areas. One way to solve this struvite precipitation problem in BNR plants is to recover phosphorus intentionally from the supernatant or sludge, through struvite crystallization.

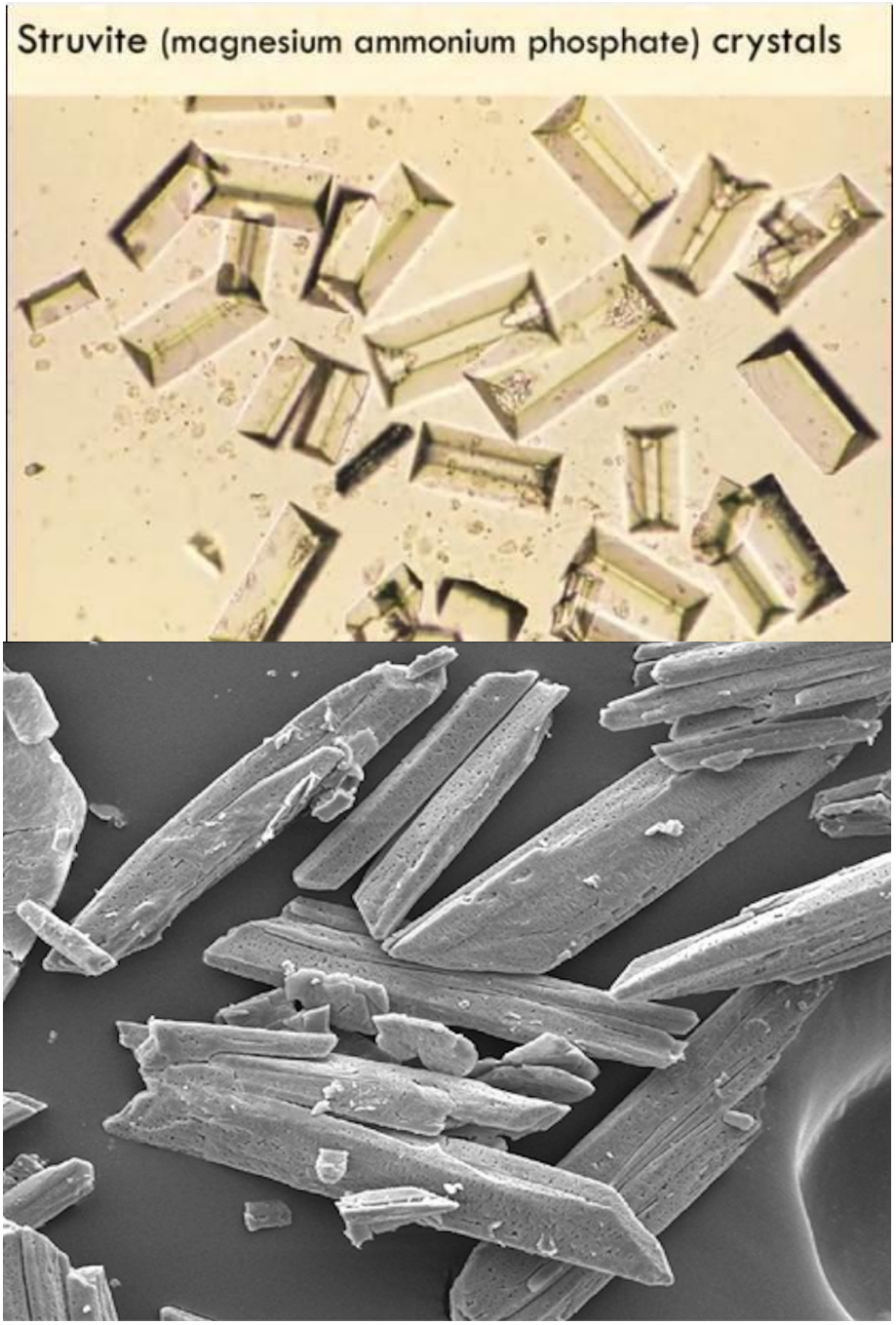

Figure 3. Struvite crystals (Orthorhombic crystal system)

This process not only alleviates the formation of unwanted struvite deposits in the digester piping and supernatant overflow and/or return lines but can also provide an environmentally benign and renewable nutrient source to agricultural industries (Yoshino, et al. 2003). In recent years, a substantial number of studies have been conducted with respect to recovering phosphorus from wastewater through struvite crystallization. These studies include process identification and performance evaluation of the struvite crystallization process, in both bench and pilot scale operations (Lee, et al. 2005, Mavinic, et al. 2007, Al Rashed, et al. 2013, Zhang, et al. 2015, Ye., et al. 2016).

The technology has also been validated in a few full-scale wastewater treatment plants, operating in different parts of the world. Being a part of this diverse research community, the Environmental Engineering Group at the University of British Columbia (UBC), has been conducting research on P-recovery since 1999 and has developed a novel fluidized bed reactor configuration that converts 80–90% of soluble phosphates into crystalline struvite (Adnan, et al. 2003). However, very little initiative has been taken to investigate the hydrodynamics of the liquid-solid fluidized bed of struvite crystals. In a fluidized bed crystallizer, the simultaneous progress of two processes, fluidization and crystallization, yields very complex phenomena. Therefore, comprehensive studies of the process hydrodynamics are required to assist in the design of an efficient reactor.

Also, a very complex phenomena occurs, as the supersaturated solution flows upward through a fluidized bed crystallizer, the liquor contacting the bed relieves its supersaturation on the growing crystals, subsequently decreasing the supersaturation in the upward direction. As a result, crystals near the bottom grow faster than those near the top of the crystallizer. Such behavior results in the variation of particle size along the height of the reactor. When a bed is composed of particles of different sizes (polydisperse), the particle size distribution is influenced by two opposite phenomena: classification and dispersion. Classification results from the movement of particles of different weights, the larger particles tend to reach the bottom of the control volume, whereas smaller particles tend to rise depending on the fluidization velocity. Simultaneously, dispersion is induced by irregular motion of the solid particles. This irregular motion is due to the collisions between solid particles (Md. Saifur, et al. 2017).

It is because of all these phenomena that a better knowledge of the mixing behavior of the particles is needed in modeling and design optimization of multi-particle, fluidized bed crystallizers. A better knowledge of bed expansion, mixing, segregation and fluidization is required to design fluidized bed crystallizers containing a wide range of particles. But there is a significant lack of research dealing with the hydrodynamics of liquid-solid fluidized bed crystallizers involving multi-particle systems.

2.1. State of the art

Focusing on struvite fluidized bed simulations using CFD (Computational Fluid Dynamics) other simulations can be found. Concretely, the (Md. Saifur, et al. 2017) has been chosen as a reference for this project. In the realization of the project they include simulations with CFD programs (ANSYS® Fluent) as well as experimental data of an existing real plant. This allows to create and dimension an identical real life CFD model and therefore, being able to approach the exact values is easier. Although the program used for the simulation is not the same one in this Master Final Project (from now on MFP), the drag models (constitutive closing equations), turbulence models, mesh type, each and every equation of transport phenomena (continuity & conservation), numeric methods and the main ideas are quite similar. The fact that they possess experimental data was the reason why it was chosen as reference.

Other simulations have been found corresponding to fluidized solids. Very few of them have polydisperse solids in their studies and / or do not speak of the same type of solid (struvite crystals). In fact, among all the other simulations, only one of them were run with struvite (Ye, et al. 2016, Ye., et al. 2016). But it is unknown what program they worked with, what numerical methods they worked with and with what experimental data they supported their simulations.

Table 1 shows a bibliographic summary about the above mentioned CFD simulations of struvite polydisperse crystals fluidization columns.

Table 1. Summary table of CFD simulations.

Reference	**Analysis**	**Program**	**Model**	**Solid/ Polydisperse**	**Pilot plant data**
Xin Ye et al. (2017)	CFD	Unknown	PBE (Population Balance Equation)	Struvite/yes	Yes
(Md. Saifur, et al. 2017)	CFD	ANSYS®	Eulerian-Granular	Struvite/yes	Yes
Xin Ye et al. (2016)	NFD	Unknown	Eulerian-Eulerian-Two Fluid Model	Struvite/unknown	Yes

In Table 1 all the above-mentioned projects are referenced. In this MFP, the analysis is going to be done by CFD (computational fluid dynamics) and the program is going to be MFiX® (open code program). The model that is going to be used is the Eulerian-Eulerian-Granular-Two-Fluid Model and the solid is going to be struvite. Also, backup data from a pilot plant will be available. Finally, the exported MFiX® results are going to be treated with ParaView® (open code program).

It should be known that the Eulerian-Eulerian-Granular-Two-Fluid model consumes a large quantity of computational requirements compared to the models shown in the previous table. But in turn it is a very complete model and very safe to use (as safe as any other model, if it's known how to work with it).

3. OBJECTIVES

The aim of this project is to model a fluidized bed of polydisperse struvite crystal particles with an open code program called MFiX®, in order to validate it against a pilot plant experimental data and also to crosscheck the results against ANSYS®.

First of all, the learning on how to perform a simulation in MFiX®, more than a goal is a necessity. And, once assimilated how to perform simulations with the tool, the following objectives have been proposed.

- To study the water volume fraction (it is complementary to the solids fraction and also known as bed voidage) profiles of the fluidized polydisperse struvite bed along all the bed height during the transient state and in the steady state. And then, check that the simulation model is correct by compare it against the experimental data (Md. Saifur, et al. 2017).
- To study the different struvite crystals heights reached in the steady state (stratification, solids density). And then, check that the simulation model is correct by compare it against the experimental data (Md. Saifur, et al. 2017).

4. MATERIALS AND METHODS: USING MFiX®

This simulation is going to be done by computational fluid dynamics (CFD) modelling, using MFiX® open code software. Computational fluid dynamics is the cheapest way in designing and running simulations and experiments, and there is no need to create or build a pilot plant. The cost of pilot plant building and repeating the process until the desired result is quite large.

The MFiX® open code software provides access to several modules that allow to simulate a high number of scenarios focusing in many different engineering cases. A brief explanation of how the software program work is explained. It is also explained what the user needs to perform a simulation. Each step is going to be explained to perform a successfully simulation, focusing on the mathematical models and on the

boundary conditions of the system. The steps that must be completed to perform a simulation are the following:

- Geometry design
- Mesh generation
- Region generation
- Impose boundary and initial conditions

The project mentioned above and referenced in Table 1 (Md. Saifur, et al. 2017) is a CFD simulation which also includes a real experimental study of a polydisperse struvite fluidized bed. Therefore, this MFP is based in their work. Because it is the best project in all the state of the art to support and check if the MFiX® is capable to reproduce the experimental data as well as ANSYS® did.

In order to perform a detailed investigation on the struvite fluidized bed system, they built a pilot experimental setup as shown in Figure 4. It is an orthophosphate crystallizer reactor with a drainage pump that drives the fluid through a fluidization column.

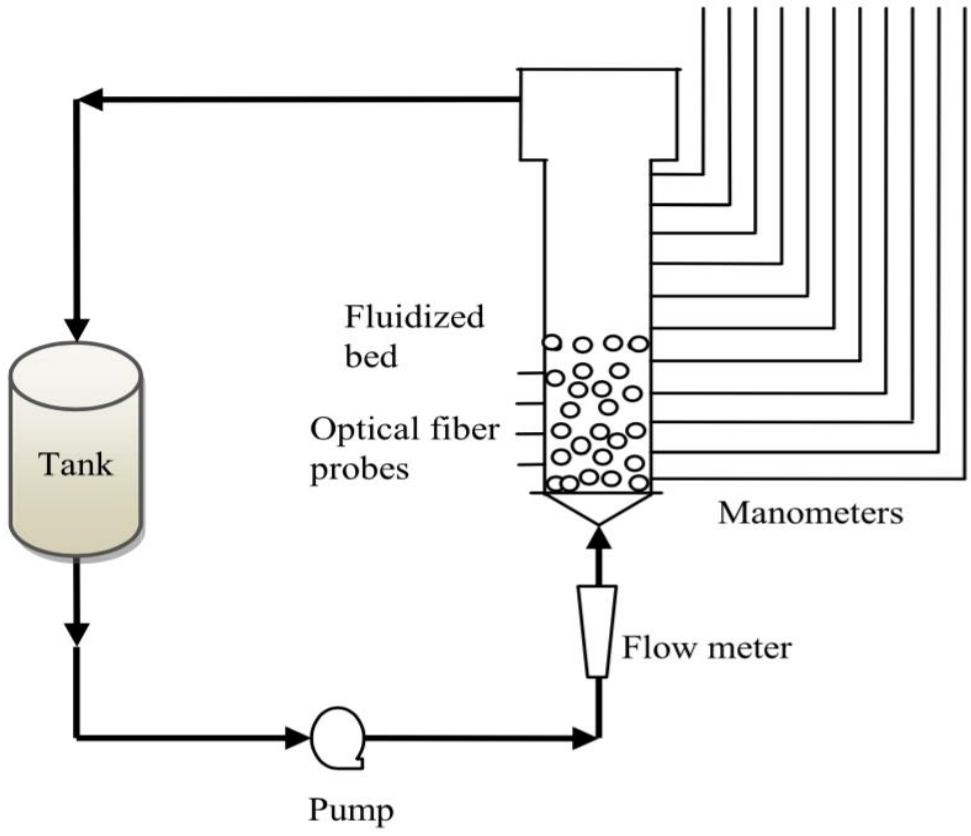

Figure 4. Pilot diagram (Md. Saifur, et al. 2017)

The fact is that they begin the study in an initial moment where there is no movement of fluid and the bed is packed at the bottom of the column. It is important to note that they only take the fluidization column as control volume to build the model, avoiding the reactor and the pump.

The cylinder (fluidized bed) of the schematic diagram shown in Figure 4, is the pattern for this work. All the column is studied as they did. It means that all the data is extracted from the column central axis (from bottom to the top), to study the profiles in height of each validation variable. The most important variable that they studied was the water volume fraction (it is complementary to the solids fraction and also known as bed voidage) in the stationary phase.

In this MFP, to check if the values of bed voidage are the correct ones, and therefore the simulation is well done, the data collected in the whole system must have the same numeric values as the experimental ones, or at least with the lowest error possible (see Figure 5).

The necessary struvite data for the simulation is shown in Table 2. This table shows a selection of struvite crystals. In their simulation a group of solids called ML was done. This group was made up of the struvite crystals, A, C and D. They also ran simulations with other groups consisting of 3 solids. Their conclusion is that the difficulty of the simulation (and the simulation time required) increases the more different solid phases are added, and the more their densities differ.

The ML group is sufficiently complex to simulate due to the similarity in the size of the particles, but also it is lighter in computation than a case with more solids. This is why it was considered as the best group of solids to simulate and validate. It will be the one shown in the following tables, and only the solids corresponding to this case will be discussed.

Table 2. Properties of different size groups of struvite crystals and experimental conditions.

Struvite size group	Solid	Density (kg/m^3)	Initial bed height (mm)	Packed bed solid volume fraction	Range of up flow velocity (mm/s)
ML	A	1,687	209	0.205	15.66 – 28.68
	C	1,687		0.205	
	D	1,677		0.205	

Struvite size group	Solid	Sieving range (mm)		Equivalent diameter (µm)
ML	A	2.00	2.20	2,233
	C	1.41	1.68	1,687
	D	1.00	1.18	1,164

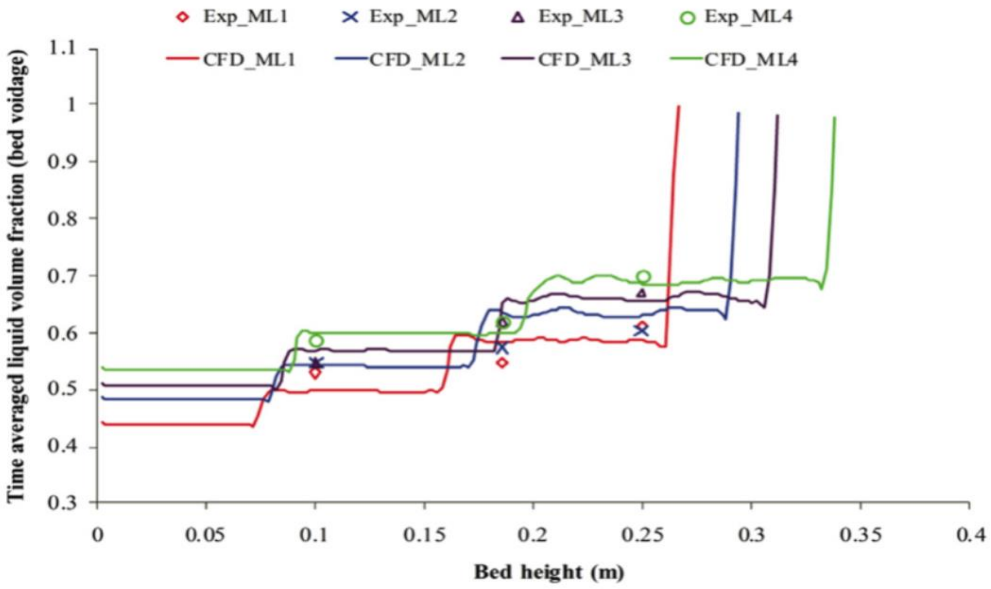

Figure 5. Time averaged liquid volume fractions along the bed height at different up flow velocities for the mixture group of ML (Md. Saifur, et al. 2017).

The data which appears in Figure 5, also explained in the 4.4 section, provides water volume fraction (is complementary to the solids fraction and also known as bed voidage) information against the bed height for different rates of water entering the system in the stationary phase. As referenced in 0, the water up-flow velocities that appear in Figure 5 are in the range of 15.66 mm/s (Exp_ML1 & CFD_ML1) to 28.68 mm/s (Exp_ML4 & CFD_ML4).

4.1. Geometry design

Before deciding which is the geometry that best defines the case to be studied, it is necessary to evaluate what information is known in order to adapt the geometry to the boundary conditions. In general, the geometries adapt to boundary conditions and not to the reverse. In this case there is no problem, since it is a cylindrical column that can be reduced by symmetry to a rectangular plane. Moreover, always is convenient to be conservative and avoid being very exact with the geometry design. In this way, studies of very complicated models can be carried out, facilitating thermodynamic and hydraulic calculations for the program. As well as saving computational time and unnecessary expense of processor requirements.

Once the boundary conditions are known and the appropriate geometry is decided, the first thing to do is to draw the geometry that is wanted to be analyzed. The whole scheme calculation domain without axis-symmetry is shown in Figure 6. To do it, MFiX® offers different tools that allow to draw any kind of geometry. It is important to recall that in this MFP and in order to optimize the project resolution, the minimum geometry is been draw. Moreover, files of another software such as ANSYS® Designmodeler, SALOME, AutoCAD, Solidworks, etc. can be imported to MFiX® database as a ".stl" extension file which is a very useful feature.

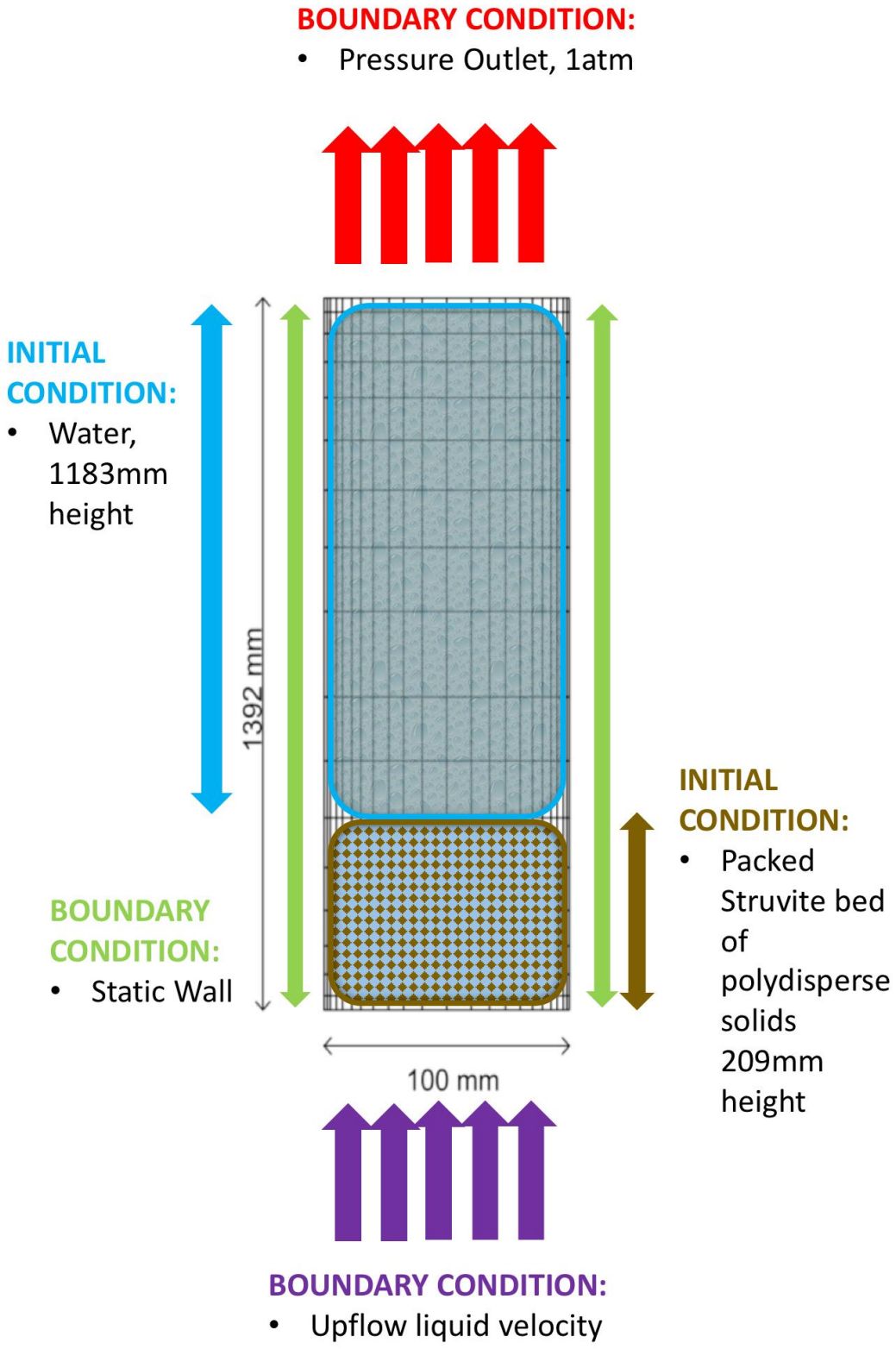

Figure 6. Whole scheme calculation domain (boundary and initial conditions are also shown)

The fluidized bed crystallizer used in this MFP has a high symmetry, and this allows to perform the project in 2D. In Figure 7 the geometry is shown. The up-flow direction is the *y* axis. The model represents the diametrical symmetry and the height of the column. This trick drastically reduces the computational time to calculate the solution. Thanks to the symmetry, the solved area is 0.1392 m^2.

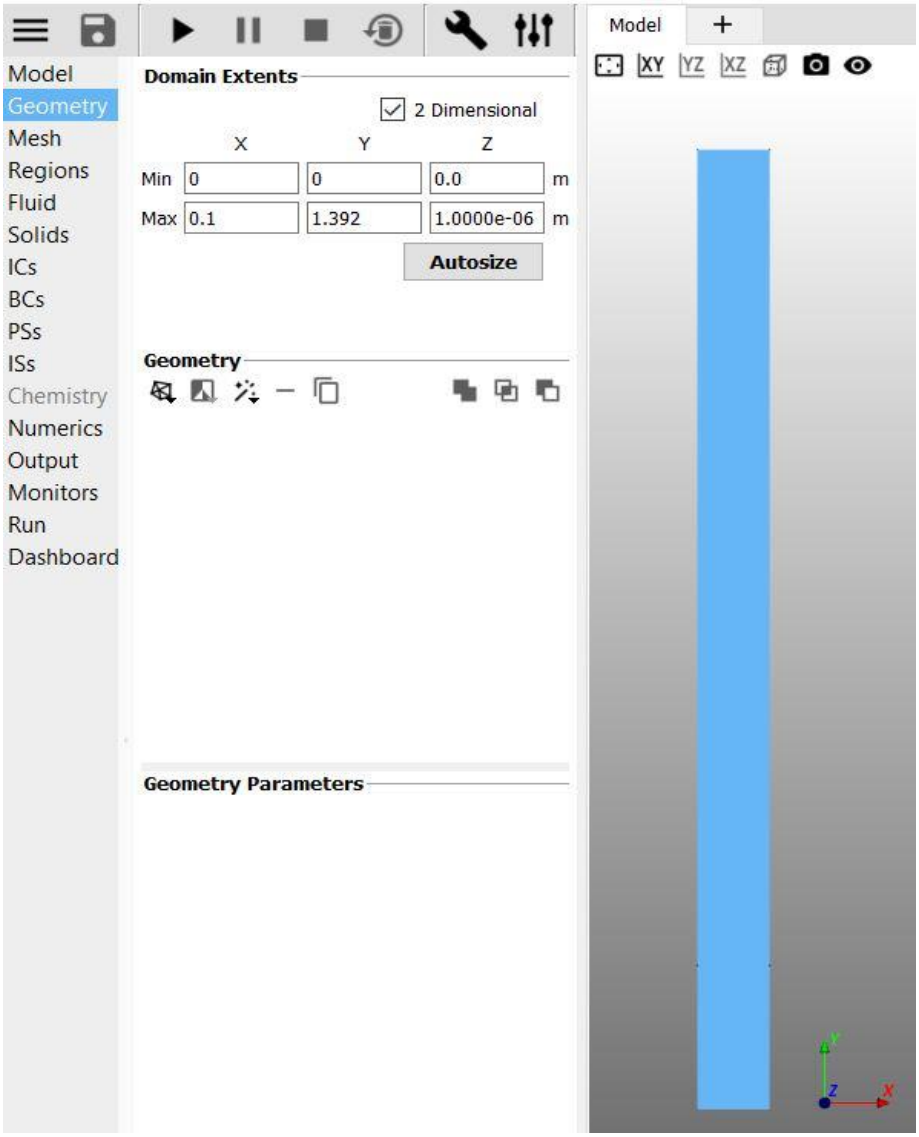

Figure 7. MFiX® snapshot. Whole geometry calculation domain (the real dimensions are given in the picture)

4.2. FAVOR Mesh generation

Once the geometry has been drawn in MFiX® or imported from other program, the system must be discretized to solve the mathematical model with the finite elements method. To solve the project without discretizing it, microscopic balances should be done, which are differential equations. But if the geometry is discretized, several finite elements are created, and the size of that thousands of finite elements are such small that those differential equations from the microscopic balances can be transformed to algebraic equations, which require less effort to be calculated and thereby optimizes the computational process.

In the fluidization column used in this study, areas that need inflation (increasing the number of nodes in the sites that is predictable that the variables are going to change more) are more complex, due to solid polydispersity. Thereby, the mesh has to be minimum (recommended) from equal size to 10 times smaller than the smallest solid of the model.

In CFD modeling, it is important to achieve results independent of the mesh size and structure. This is why in this project extremely fine meshes are used, given that thanks to the great computational capacity that is possessed, it will not be a great temporal challenge "to go over nodes". The concept of "to go over nodes" is relative, since a perfect simulation can ensured by placing extremely small nodes, but it is not necessary, probably the same results could be achieved with a much smaller number of nodes. But this last one supposes to generate feasibility studies that take more time than the computational time itself.

Keep in mind that MFiX® uses a meshing method different from the common ones. Specifically, it uses the FAVOR (fractional area / volume method). Which is a full orthogonal meshing method. The simplicity granted by the FAVOR for modeling complex geometric regions is very well valued, given that often when meshes are made in alert zones (in areas with large geometrical variations, such as areas with curves or very small structures) the mesh creation can cause some trouble. In this case no trouble can appear due that, when these difficulties appear the created cells are cut, and the centroid is

moved to a new position (FLOW-3D, 2019). In Figure 8 the used mesh is shown. These dimensions in Figure 8 are the real ones and so that the user can visually see how the nodes are formed. A mesh picture with zoom is also shown in the right part of Figure 8. It can be seen how the nodes have been carefully made to fulfill the aspect ratio as best as possible; that is, trying to generate completely squared nodes (with the edges of the same size or as similar as possible).

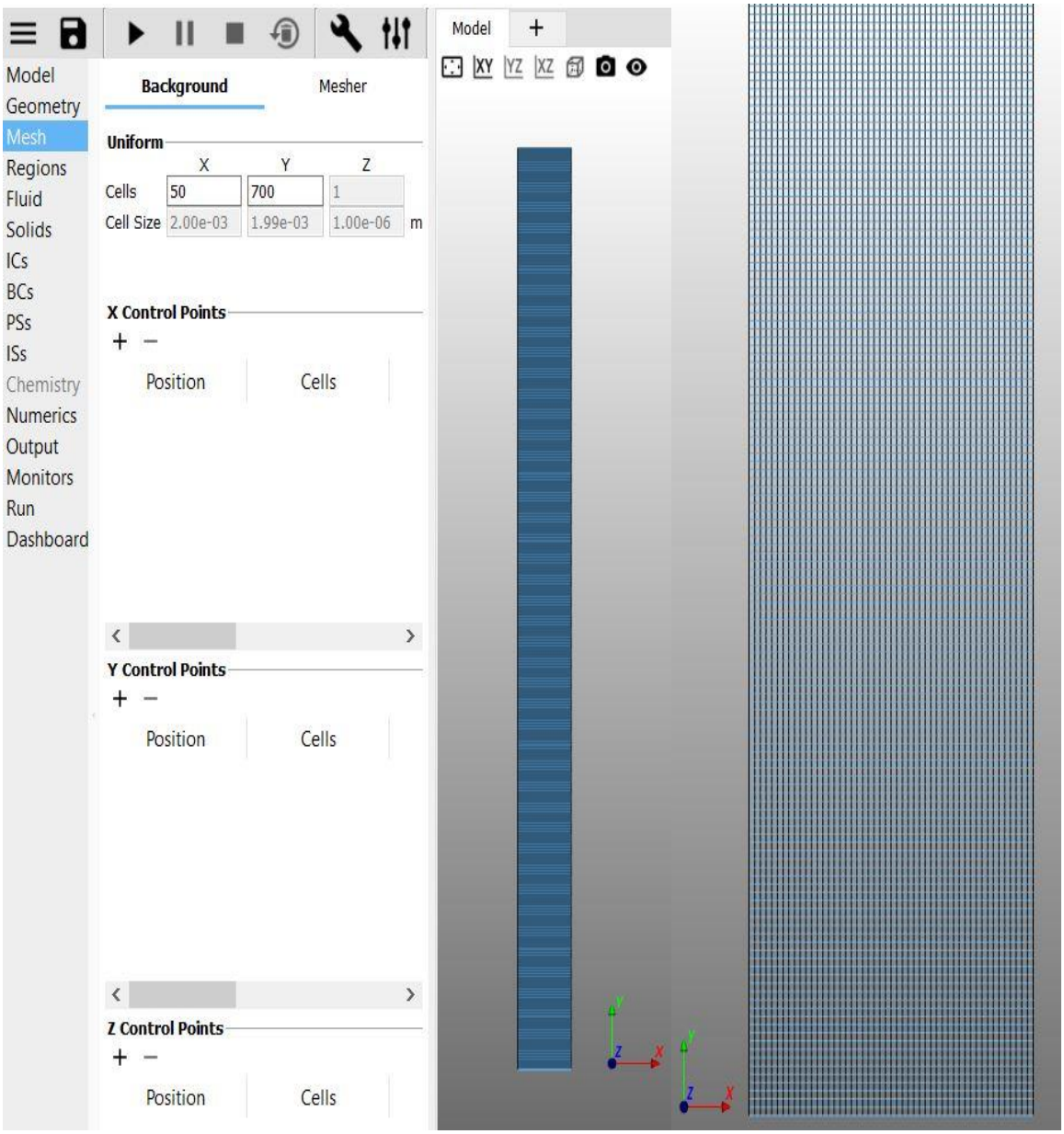

Figure 8. MFiX® snapshots. Whole meshed geometry calculation domain and zoom picture

4.3. Region generation

The working regions must be defined in MFiX®, so that it can be indicated later where the existing solids are located in the model, the fluid, the initial conditions, the boundary conditions in each of the regions, etc. The following snapshot Figure 9 will show the MFiX® GUI at the time of entering regions. The solid bed region has been selected, so that the reader gets an idea of the inputs needed to define it.

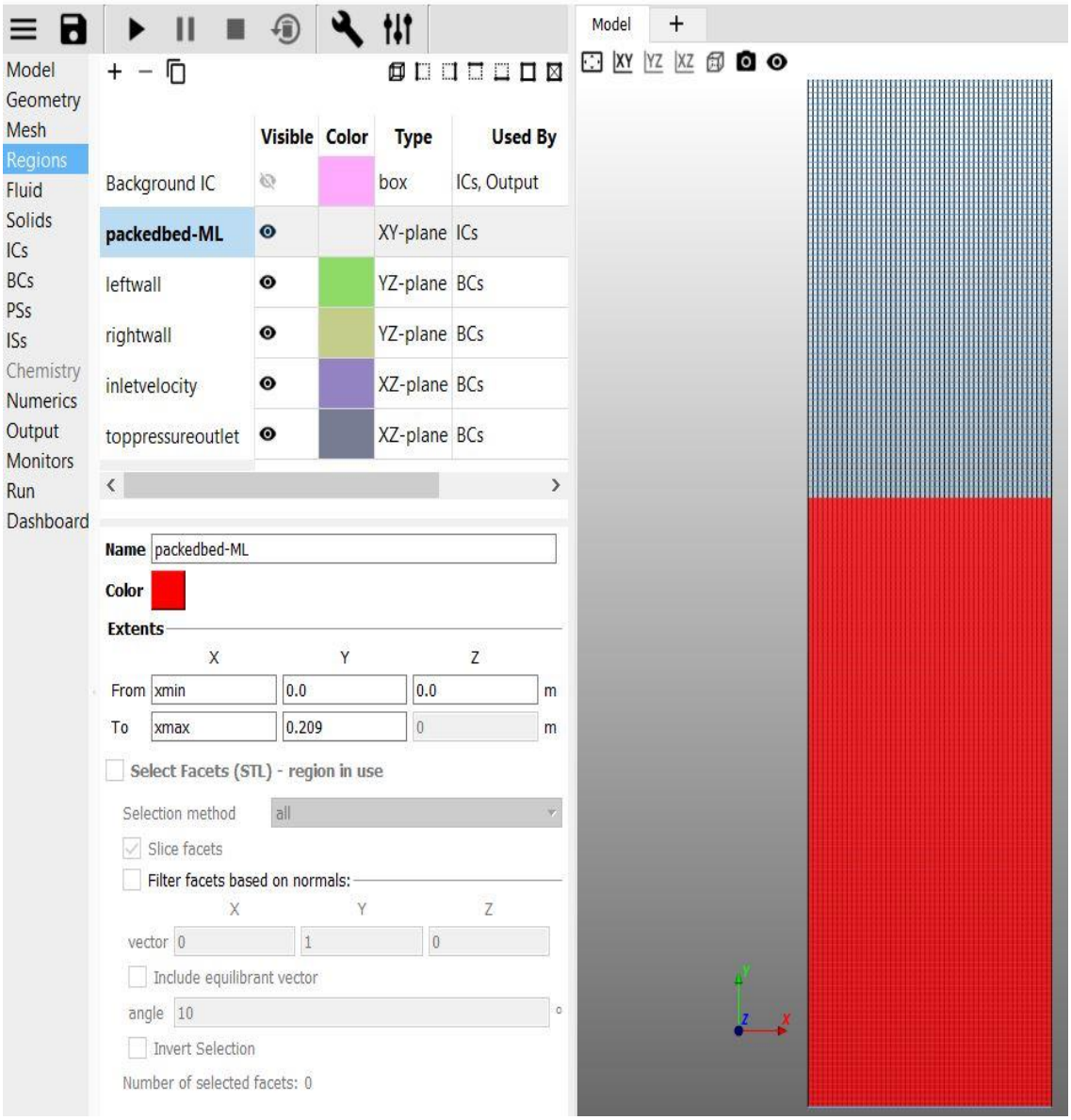

Figure 9. MFiX® snapshot. Domain of regions. Selected "packedbed-ML").

In Figure 9 there is a zoom created to let the reader see the selected region. The complete domain is not shown because nothing would be seen in specific, due that the rest of the regions are edges. That is, the "leftwall" and "rightwall" are the walls of the fluidized column. The "top pressure outlet" corresponds to the upper exit and the "inletvelocity" corresponds to the lower portion where the fluid will enter in an upward direction. But if the reader goes into detail, a region called "Background IC" can be seen. This region refers to everything that exists in the model. It simply refers to all the points from which it is going to be extracted or from where it will be possible to extract information from the model.

4.4. Boundary and Initial conditions

The boundary conditions are as shown in Figure 6:

- Outlet pressure condition (1 atm)
- Ambient temperature of 20 ºC is selected as input
- No slip walls
- Inlet velocity conditions (4 different case studies):

    1# 18.26 mm/s

    2# 22.7 mm/s

    3# 25.29 mm/s

    4# 28.68 mm/s

The initial conditions are also shown in Figure 6:

- Packed struvite bed of polydisperse solids (209 mm) height
- Water (1183 mm) height

- If a homogenous initial pressure is not selected in the whole system, the program calculates a first hydraulic profile, generating an adequate vertical integration to the flow / pressure contour data. In this case, no initial pressure is selected.

The measurements made in the pilot plant are taken at the heights of 0.10 m, 0.19 m and 0.25 m. To validate the data in those points shown in Appendix (Tables A1 to A8), they should not exceed the relative error of 5 %.

5. SIMULATION SETUP

MFiX®-TFM (Two-Fluid Model) is a model where solids and liquids are treated as an interpenetrating continuous phase, that is, as if they were only one phase. But not to create a single phase from both, since this approach would not be real or logical. Given this last premise, the concept of phasic volume is generated. With this concept, none of the phases can occupy the volume of the other. These volume fractions are continuous functions with respect to space and time.

$$Vf(x,t) \tag{1}$$

These phasic volume fractions are included in the numerical balances of CFD. That is, in the equations of conservation (momentum), and continuity (energy and mater). These conservation and continuity balances are derived to obtain a set of similar equations for all the phases. Once the equations are obtained, they are closed with constitutive relays (empirical equations with empirical data) and / or for granular flows

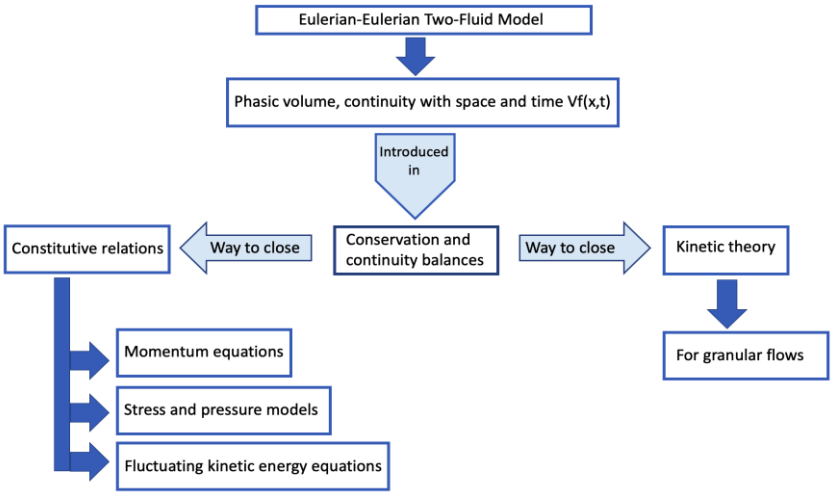

Figure 10. Summary, application of mathematical models

(kinetic theory). Figure 10 shows a schema that indicates how to use the numerical models.

When establishing a mathematical model in CFD, it must be taken into account that equations for the fluid and for the solids will be generated separately. Thereby, there will be balances of matter, momentum and energy transfer, specifics for the fluid and for the solid. Highlighting the energy transfer equation in solid phase, it will be called “fluctuating kinetic energy equation”. It models the fluctuating energy generated from solids by the kinetic theory of granular flow.

In the Eulerian-Eulerian models, each solid phase is considered a different phase. Thus, an equivalent number of continuous equations (matter and fluctuating kinetic energy transfer) and impulse equations (momentum) are included.

The equations of continuity and momentum conservation mentioned must be closed as indicated above, and this will be done through interaction equations and stress equations (constitutive equations).

The equations and models that MFiX® discretizes for each node generated in the meshing step are the following.

5.1. Continuity for liquid and solids

$$\frac{\delta}{\delta t}(\alpha_l \rho_l) + \nabla.(\alpha_l \rho_l v_l) = 0 \quad (2)$$

$$\frac{\delta}{\delta t}(\alpha_{si} \rho_{si}) + \nabla.(\alpha_{si} \rho_{si} v_{si}) = 0 \quad (3)$$

5.2. Momentum for liquid and solids

$$\frac{\delta}{\delta t}(\alpha_l \rho_l v_l) + \nabla.(\alpha_l \rho_l \aleph_l) = -\alpha_l \nabla P + \nabla Z_l + \alpha_l \rho_l g + \alpha_l \rho_l F_l + \sum_{i=l}^{n} k_{si,l}(v_{si} - v_l) \quad (4)$$

$$\frac{\delta}{\delta t}(\alpha_{si} \rho_{si} v_{si}) + \nabla.(\alpha_{si} \rho_{si} \aleph_{si}) = -\alpha_{si} \nabla P + \nabla Z_{si} - \nabla P_{si} + \alpha_{si} \rho_{si} g + \alpha_{si} \rho_{si} F_{si} + k_{si,l}(v_l - v_{si}) + \sum_{m1;m\neq 1}^{n} k_{sm,si}(v_{sm} - v_{si}) \quad (5)$$

5.3. Kinetic energy for solid phases

$$\frac{3}{2}\left[\frac{\delta}{\delta t}(\alpha_{si} \rho_{si} \Tf_{si}) + \nabla.(\alpha_{si} \rho_{si} v_{si} \Tf_{si})\right] = \left(-P_{si}\hat{\mathrm{I}} + Z_{si}\right): \nabla v_{si} + \nabla(k_c \nabla \Tf_{si}) - \gamma_{si} + Q_{l,si} \quad (6)$$

Where, $\left(-P_{si}\hat{\mathrm{I}} + Z_{si}\right)$ is the generation of energy by the stress tensor.

The following equations are responsible for closing the momentum and continuity balances using empirical models. They can provide relationships for:

- The stress tensors of different solid phases Z_{si}.
- For the contact pressures of solids $\boldsymbol{P_{si}}$.
- For momentum exchange coefficients $\boldsymbol{k_{si,l}}$ and $\boldsymbol{k_{sm,si}}$
- For the parameters of the fluctuating kinetic energy equation, $\boldsymbol{k_c}$ and γ_{si}.

5.4. The stress and pressure for both liquid and solids

$$Z = \alpha\mu(\nabla v + \nabla v^T) + \alpha(\lambda - \frac{2}{3}\mu)\nabla v\hat{\mathrm{I}} \quad (7)$$

Where the $\mu = (\mu_s, \mu_l)$ and $\lambda = (\lambda_s, \lambda_l)$ are the shear and bulk viscosity of the phases, respectively. The solid shear viscosity, μ_s, is composed of three different parts. The first part is the contribution from collisions, which is significant in dense flows. The second one is the kinetic term, which dominates in dilute flow. The last one is the frictional viscosity. Thus, the solid shear viscosity can be written as follows (Gidaspow 1994)

$$\mu_s = \mu_{s,col} + \mu_{s,kin} + \mu_{s,frict} \tag{8}$$

$$\mu_{s,col} = \frac{4}{5}\alpha_s \rho_s d_v g_{o.ss}(1 + e_{ss})\left(\frac{\Theta_s}{\Pi}\right)^{0.5} \tag{9}$$

Being d_v the diameter of particles, e_{ss} the restitution coefficient due to particle collisions, Θ_s the granular temperature, and $g_{o.ss}$ the radial distribution function expressed by (Gidaspow 1994).

$$g_{o.ss} = \frac{3}{5}\left[1 - \left(\frac{\alpha_s}{\alpha_{s,max}}\right)^{\frac{1}{3}}\right]^{-1} \tag{10}$$

Where, $\alpha_{s,max}$ is the maximum solids volume fraction (or packing) in the bed. The kinetic and the frictional viscosities are expressed as follows.

$$\mu_{s,kin} = \frac{10 d_v \rho_s \sqrt{\Theta_s \Pi}}{96\alpha_s(1+e_{ss})g_{o.ss}}\left[1 + \frac{4}{5} g_{o.ss}\alpha_s(1 + e_{ss})\right]^2 \tag{11}$$

$$\mu_{s,fr} = \frac{P_s \sin\theta}{2\sqrt{I_{2D}}} \tag{12}$$

Where, P_s is the solids pressure, θ is the angle of internal friction, defined as the angle measured between the normal force and resultant force that is attained when failure

just occurs in response to a shearing stress; finally, I_{2D} is the second invariant of the deviatoric stress tensor.

$$P_s = \alpha_s \rho_s \text{Ŧ}_s + 2\rho_s(1 + e_{ss})\, {\alpha_s}^2 g_{o.ss} \text{Ŧ}_s \quad (13)$$

The solid bulk viscosity λ_s is the resistance of the granular particles to compression and expansion and is given by (Lun, et al. 1984):

$$\lambda_s = \frac{4}{5}\alpha_s \rho_s d_v g_{o.ss}(1 + e_{ss})\left(\frac{\text{Ŧ}_s}{\Pi}\right)^{0.5} \quad (14)$$

5.5. Parameters for the kinetic energy equation

The diffusion coefficient for the energy fluctuations of a solid phase (kc) is given by (Drew 1983)

$$k_c = \frac{150\rho_s d_v \sqrt{\text{Ŧ}_s \Pi}}{384(1+e_{ss})g_{o.ss}}\left[1 + \frac{6}{5} g_{o.ss}\alpha_s(1 + e_{ss})\right]^2 + 2{\alpha_s}^2 \rho_s d_v g_{o.ss}(1 + e_{ss})\left(\frac{\text{Ŧ}_s}{\Pi}\right)^{0.5} \quad (15)$$

The collisional dissipation of energy γ_s can be expressed by (Drew 1983) as

$$\gamma_s = \frac{12(1-{e_{ss}}^2)g_{o.ss}}{d_v\sqrt{\Pi}} \rho_s {\alpha_s}^2 {\text{Ŧ}_s}^{1/2} \quad (16)$$

The dissipation of energy fluctuations due to the transfer of the kinetic energy of random fluctuations in the particle velocity from the solid phases to the liquid phase is given by (D.G. 1987, Sudaporn, et al. 2016)

$$Q_{l,s} = -3k_{l,s}\text{Ŧ}_s \quad (17)$$

5.6. Momentum exchange coefficients

There are many solid drag laws, among them, the most relevant and used by CFD simulation programs such as MFiX® will be shown below. These laws are empirical, so it has to be considered when to use them. These considerations will depend on the system to be simulated and the characteristics of the system itself. Some empirical models proposed are:.

- In case of high void fractions (fluid volume fraction) $\alpha_l \geq 0.8$ (Wen and Yu 1966)

$$K_{l,s} = \frac{3}{4}\frac{24}{\alpha_l Re_s}[1 + 0.15(\alpha_l Re_s)^{0.687}]\frac{\alpha_s\alpha_l\rho_l|v_s - v_l|}{d_v}\alpha_l^{-2.65} \quad (18)$$

$$Re_s = \frac{d_v|v_l - v_s|\rho_l}{\mu_l} \quad (19)$$

- General model (Gidaspow 1994) to cover all fluid volume fraction ranges. It is the extended method of Ergun (Ergun 1993) and is coherent with that of Wen (Wen and Yu 1966)

$$K_{l,s} = 150\frac{\alpha_s(1-\alpha_l)\mu_l}{\alpha_l {d_v}^2} + 1.75\frac{\alpha_s\rho_l|v_s-v_l|}{d_v} \quad (20)$$

- Other methods are proposed (Syamlal and O'Brien 1988) based on methods of terminal velocity of a particle in a fluidized or fixed bed,

$$K_{l,s} = \frac{3C_D}{4{u_{r,s}}^2}\frac{\rho_l|v_s-v_l|}{d_v}(\frac{Re_s}{u_{r,s}})\alpha_s\alpha_l \quad (21)$$

$$C_D = (0.63 + \frac{4.8}{\sqrt{\frac{Re_s}{u_{r,s}}}})^2 \quad (22)$$

The correlation of the terminal velocity $u_{r,s}$ can be calculated with the models of dump-speed (Garside and Al-Dibouni. 1977), but it is not going to go into detail, because they are not used in this model. Other models (Gidaspow 1994, Wen and Yu 1966) are highly reliable for the simulation presented in this work.

A part of the conservation and continuity equations. There are extremely complex numerical methods that are used to maintain convergence in the calculation system. It is not that these forces a result even if it has no physical sense, but that it is about debugging calculation errors generated for example by a complex geometry. When debugging these errors that are known to appear, no physical reality is removed from the simulated system, but helps to advance in it. It must be said that in order to perform the simulation, a very complex sensitivity analysis of them has had to be carried out before reaching the one that fits to the studied model.

6. RESULTS AND DISCUSSION

As described above, the variables that have served to validate the model are displayed in Figure 11, Figure 12 and Figure 13. The variable that has been used for validation in this work is the liquid volume fraction (**c**omplementary to the solids fraction**),** also known as bed voidage. Therefore, the following information will show ANSYS® data against experimental data, MFiX® data against experimental data and ANSYS® data against MFiX® data. Another very interesting variable to analyze is the bulk density of the fluidized bed. In this way, besides being able to visualize the relative position of each package of solids in a joint picture, they can also be viewed individually. The information will be displayed in graphics and also as vector pictures. The bulk density is defined as:

$$\rho_{bulk} = \rho_s(1 - \alpha) \qquad (23)$$

Where α is the interstitial porosity of the bed and ρ_s is the solid density. This means that the information of bulk density will be shown for each solid type (A, C and D).

The bulk density of a particle is inversely related to the porosity of the same particle, the more pore space in it the lower the value for bulk density. But in this case the particles are considered spherical and without internal porosity, so the bulk density will be defined only as a function of volume occupied by these particles in the bed, considering the volume occupied by the fluid as the porosity (ρ_s) of the bed. And this value will be characteristic, because it will give information about how compact the particles are in the steady state and during the transient state.

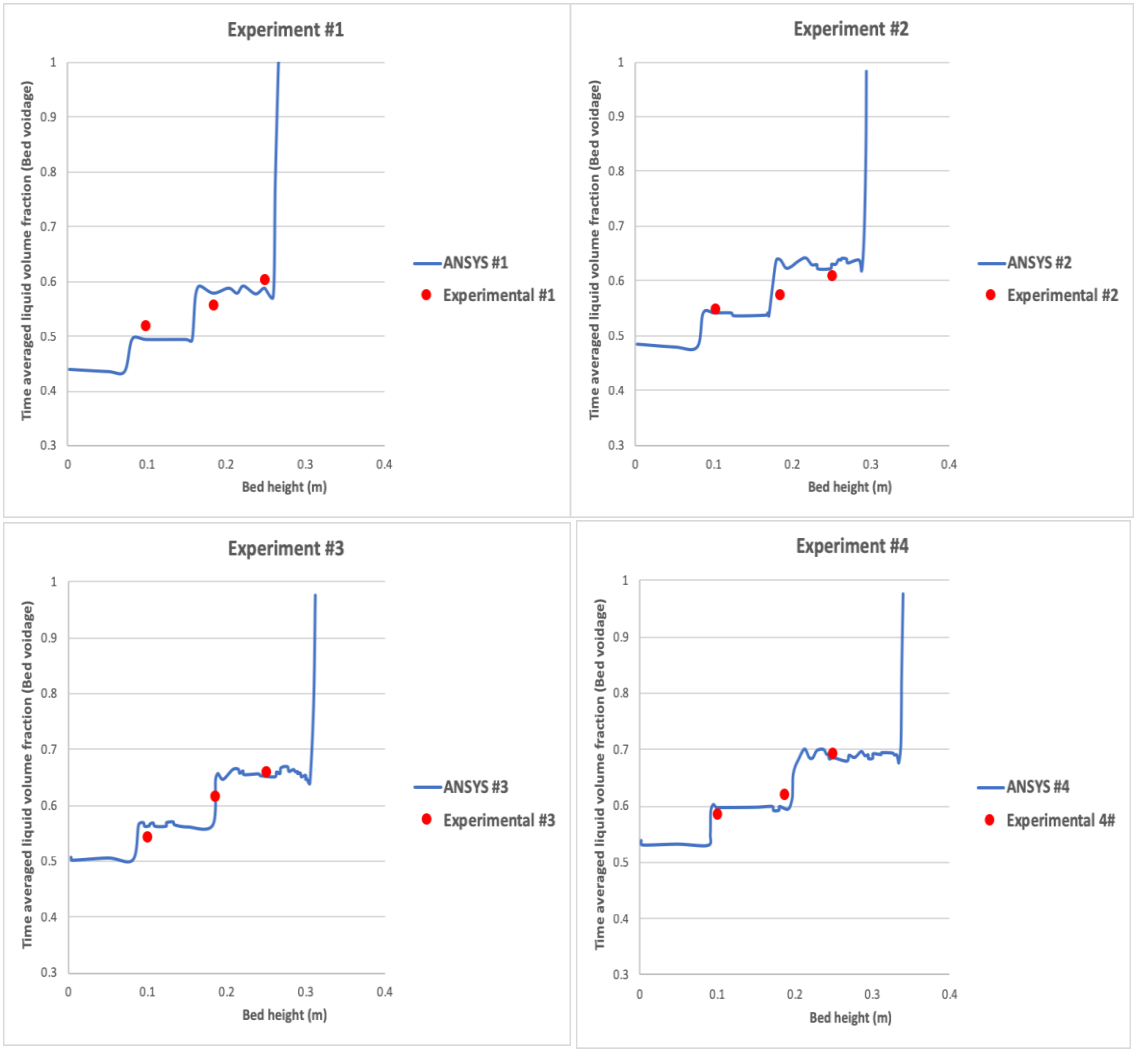

Figure 11. ANSYS® & Experimental data. Time averaged liquid volume fraction (bed voidage at 120 s) against bed height. Experiments 1#, 2#, 3#, 4#.

Figure 11, shows the fluid volume fraction against the height of the fluidization column for the four experiments performed. Each of the experiments corresponds to an input velocity as explained in the section 4.4.

ANSYS® simulation results fit to the experimental results. The errors related to each height of data collected in the pilot plant against the ANSYS® data at the same heights, are shown in Table A.1, Table A.3, Table A.5 and 0 of the Appendix. The maximum ANSYS® error is 6.09%.

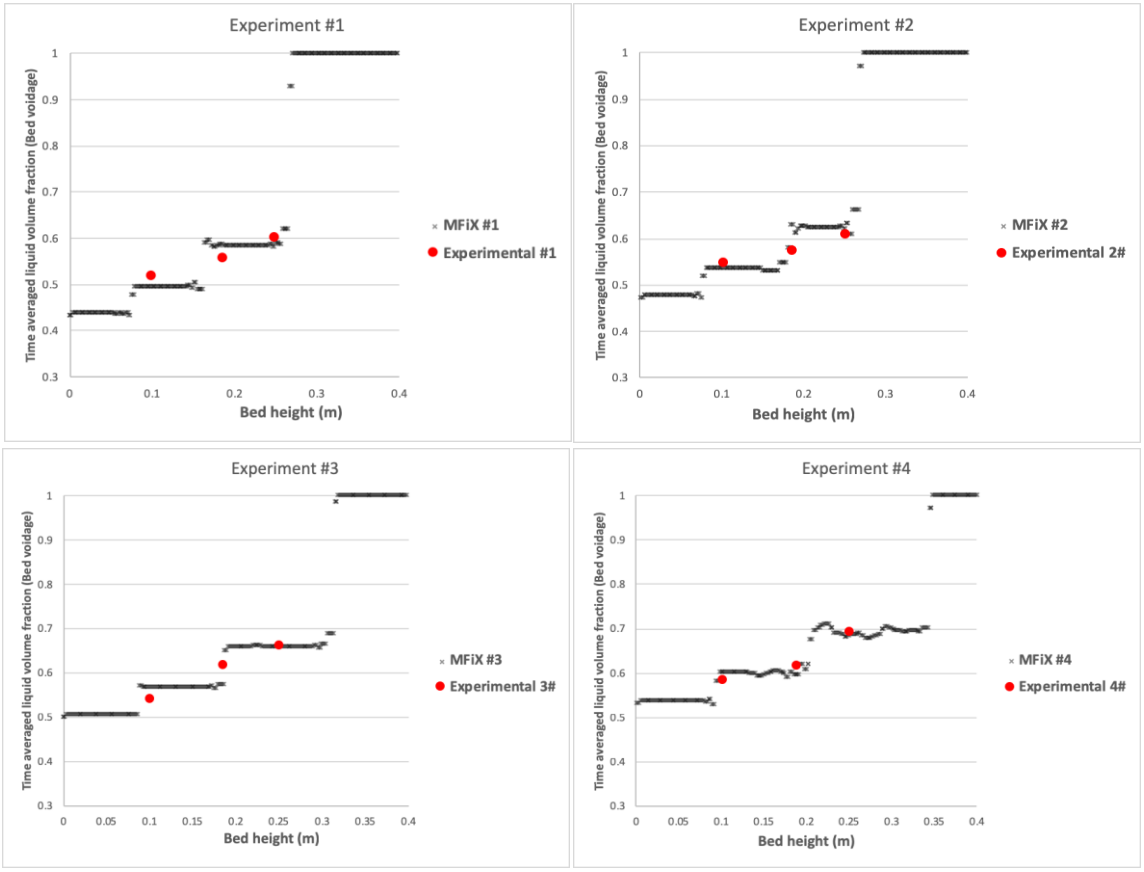

Figure 12. MFiX® & Experimental data. Time averaged liquid volume fraction (bed voidage at 120 s) against bed height. Experiments 1#, 2#, 3#, 4#.

Figure 12 shows how MFiX® values are adjusted to the experimental data. The errors related to each height of data collected in the pilot plant against the MFiX® data at the same heights are shown in the Appendix (Table A.2, Table A.4, Table A.6 and Table A.8). The maximum MFiX® error is 3.76%. Once the results/data extracted from ANSYS® are shown against those of MFiX®, the concepts of extracted information will be developed, and the results will be explained.

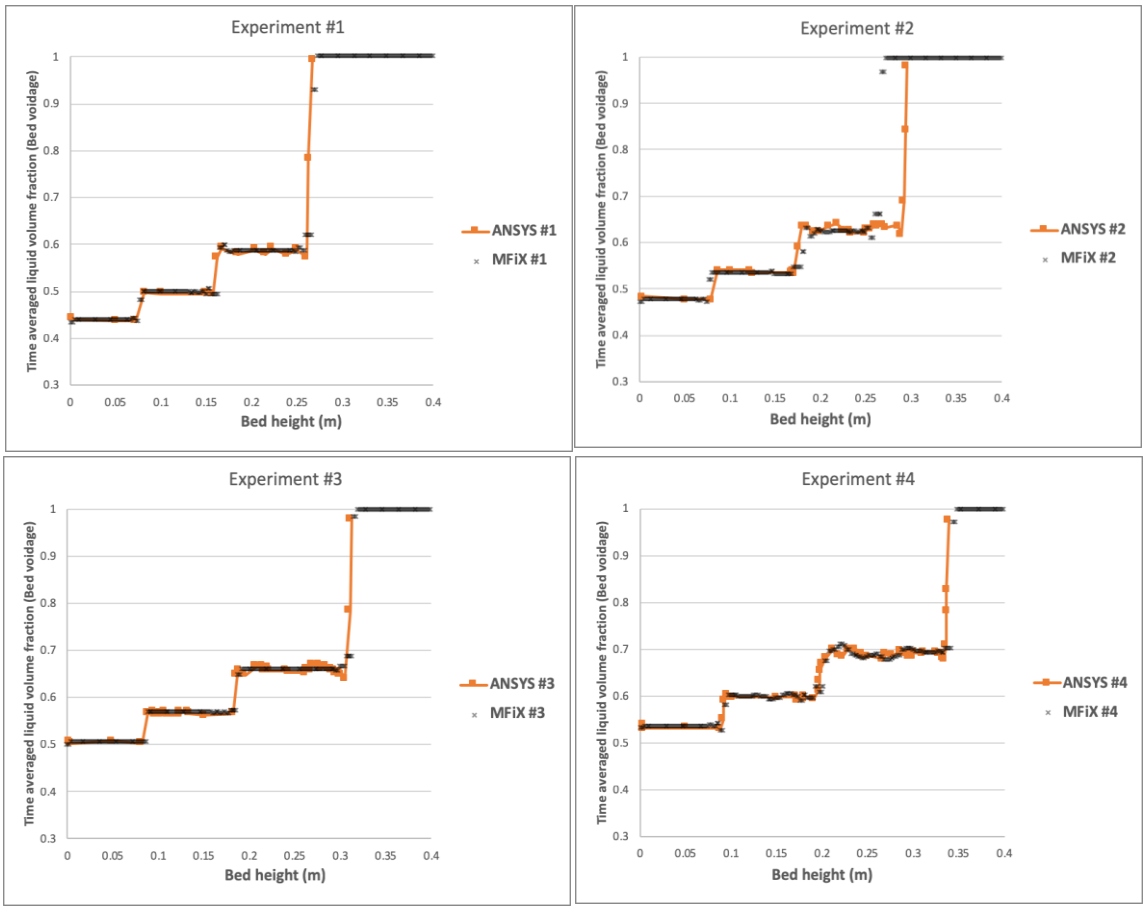

Figure 13. ANSYS® & MFiX®. Time averaged liquid volume fraction (bed voidage at 120 s) against bed height. Experiments 1#, 2#, 3#, 4#.

Once the results of ANSYS® and MFiX® are compared in Figure 13, the deviations between simulated models can be evaluated. Both CFD models carried out in 2 totally different programs, with different constitutive models and with totally different meshing, drop more or less the same results, with a 2.24% maximum difference. The deviations between the results of the simulations are minimal, and in turn are deviated in a very similar way between them and the results of the pilot plant. This could indicate that it would be good to re-take experimental data to verify that they were taken in a steady state. If the experimental data returned to give the same results, it could be said that both programs have the same numerical limitations.

In the world of simulations, the errors between experimental data and simulations that are less than 5% are considered accepted and those less than 3% are considered

successful. In this case the points studied in the MFiX® model coincide with an overwhelming accuracy with the reference experimental data (Md. Saifur, et al. 2017).

Once the model has been validated with the experimental data and compared to the data extracted with another computational fluid dynamic simulator, the obtained results are explained.

Each of the simulation runs started with rest particles and completely mixed. Therefore, once the fluidization started, they experienced a random movement in a transient time and finally reached a steady state with a stable particle size distribution. It is commonly observed that when a multiparticle system is fluidized, the particles experience both classification, due to gravitational force, and dispersion due to irregular movements of particles that are being fluidized (Md. Saifur, et al. 2017, Epstein 2003). Therefore, complete and well mixed segregation are the two extreme conditions that are generally observed in the crystallizer bed, with a polydisperse system of solids being fluidized.

A steady-state condition in terms of particle size distribution is achieved in the simulations within 60 s to 70 s. Therefore, the bed properties averaged over time, presented in this section, represent the average values found during the steady state operating time period at 120 s to be conservative. The time averaged liquid volume fraction (bed voidage) for different liquid surface velocities is shown in Figure 11, Figure 12 and Figure 13, where it is found that the crystallizer bed is separated into 3 layers in each simulation run. This means that the three size groups were segregated, with the largest particles occupying the bottom of the column, the smaller particles concentrated at the top and the medium sized particles occupying the middle section.

However, instead of a sudden change from one segregated pack to other segregated pack of solids (interface), gradual changes were observed in the water volume fraction simulated between two successive layers of particles. This means that a thin mixing zone may have developed between two successive layers of completely segregated particles. The mixing zone is clearly evident between the upper and middle section of the crystallizer bed, especially at a higher surface liquid velocity 4# experiment. These small

non-sudden changes imply almost a non-complete segregation of particles in the fluid bed in those points between segregated solid layers.

In a multiparticle system, when the particles differ only in size, the larger particles will always separate to some degree below the smaller ones, unless the size difference is small enough or when, complicating factors, such as bulk circulation or hydrodynamic instability are large enough, to mix the two particle species completely.

The bed segregated heights increased with increasing up flow liquid velocities. The proportional increasing of the height for each up-flow velocity can be seen in Figure 11, Figure 12 and Figure 13. This is due to the terminal velocity reached by a particle of determined diameter and density for each up-flow velocity. It must be borne in mind that the particles in this case cannot be individually evaluated as a fluidized solid with its unique terminal velocity. This terminal velocity must be evaluated according to a pack of solids that collide continuously between them.

This means that there are particles that are arranged on top of others in the pack of solids. Thereby, the loss of pressure / driving force / back pressure that the fluid generates on the particles is not the same in those particles that are located in the lower portion in verse to which are located in the upper portion. Very likely some particles will be supported over the others by this cause. The clearest example is that the 3 different large segregations of struvite solids can be seen (because of the diameter differentiation) occupying each one a large space of the crystallizer.

The following equation shows the variables which the terminal velocity depends on.

$$V_t = \sqrt[2]{\frac{2mg}{\rho A C_d}} \tag{24}$$

This equation represents the terminal velocity for an discrete particle, where V_t represents terminal velocity, m is the mass of the particle, g is the gravity acceleration, C_d is the drag coefficient, ρ is the density of the fluid through which the particle is falling, and A is projected area of the particle (orthogonal to the flux). Focusing on A, the fluid does not collide in the same way to each solid, thereby the loss of driving force against them is not the same, for that reason some are supported on others in a steady state. Reaching a state of minimum collisional energy.

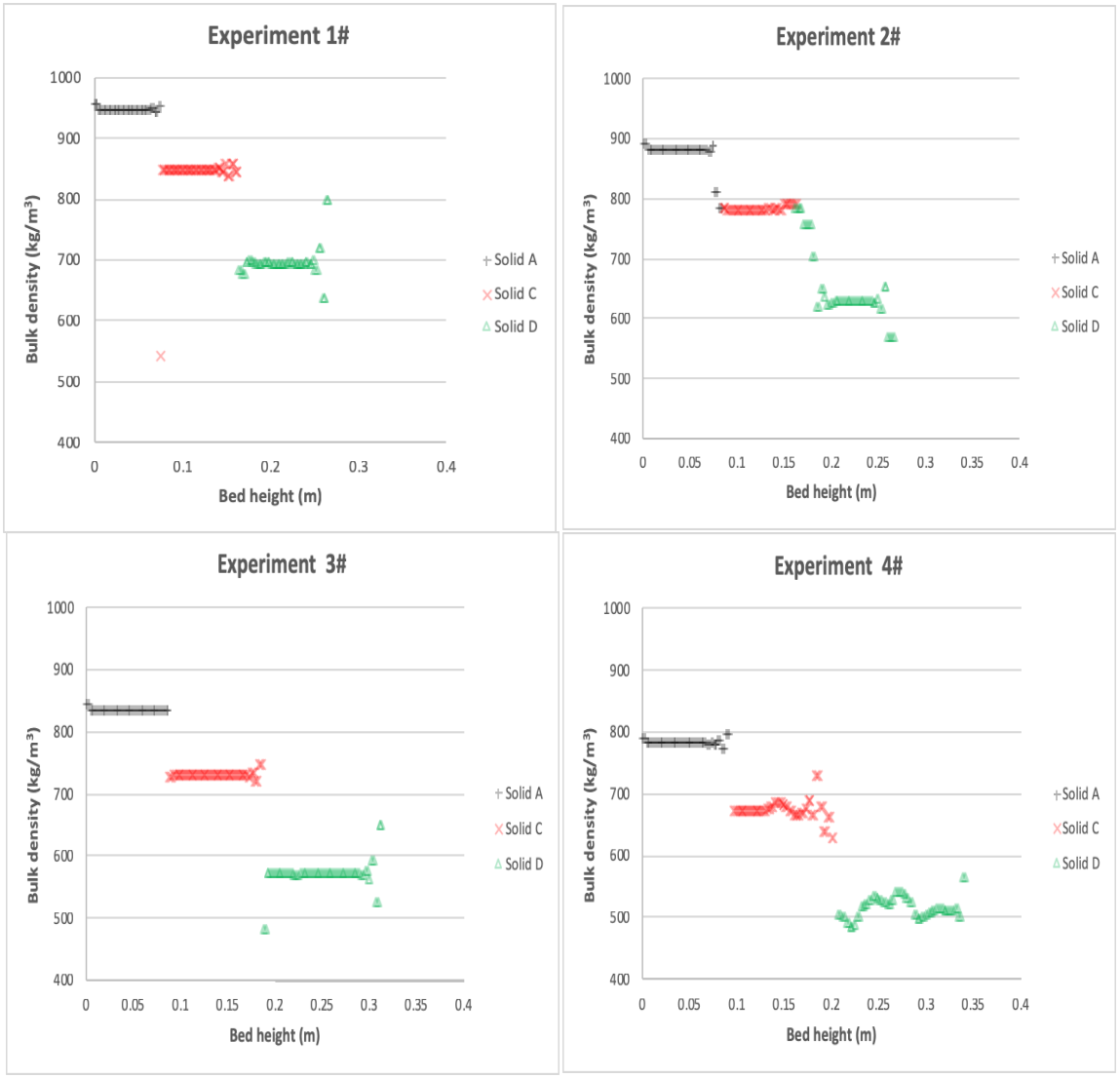

Figure 14. MFiX®. Bulk density against bed height at 120 s. Experiments 1#, 2#, 3#, 4#

The axial distribution of particles in multi-particle systems can also be described based on stability considerations. The compositions of different layers adjust themselves in order to minimize the potential energy of the suspension. These conditions are

satisfied when the slurry density at the bottom layer is maximum (when steady state is reached) and agrees with previous data (Hoffman, Lapidus and Elgin 1960).

Figure 14, shows the behavior of the different groups of solids, A, C and D, representing the bulk density in each bed height for each velocity case study 1#, 2#, 3# and 4#. In this way it is possible to evaluate the segregation of the particles according to the diameter in a simpler way and the sudden change from one segregated pack to other segregated pack of solids (interface) is easier to differ.

In the interface zones created at steady state between the particle segregated layers (A-C, and C-D), bulk density results vary randomly, visually generating those mixing zones that do not reach a stationary state as the rest of the system. Due to these non-stationary mixing areas, it can be concluded that there is no complete segregation of the bed, since the differentiation of particle sizes exceeds a critical value that does not allow perfect stationary mixing to be carried out.

As said above, in those type of multiparticle system, when the particles differ only in size but not in density, the larger particles will always separate below the smaller ones, unless the size difference is small enough or when, complicating factors, such as bulk circulation or hydrodynamic instability are large enough to mix the two particle species completely. This pattern is characteristic of smaller particles given their greater mobility within a given fixed volume. If the fluidization behavior is checked, it can be visualized how the larger particles (A group) do not have these characteristic mixing zones either in the lower portion of their pack. But if the upper part of the pack is checked, the effect can be seen. However, as the particle size decreases, this effect becomes clearer, it can be seen in Figure 14. Concretely the D particles generate oscillations of bulk density in those solid pack areas.

In summary, the effect of segregate stability in the steady state, seems to decrease for a same time step when the water velocity injection is higher, it can be seen in Figure 14. This can be due that the solids retain more fluctuating energy given the random collisions between solids and against the fluid at higher speeds. Thereby, the solids do not reach their state of minimum energy so fast, because the collisions increase when increasing their mobility and the amount of energy to liberate is higher.

It is good to know that speed plays an authoritative role in the fluidization of the beds against particles of smaller diameter and / or density for a certain velocity range and for a certain fluid viscosity. Hydrodynamics of fluidized beds are very complex phenomena and include a large amount of constitutive relationships, but the fact of being able to find the relationships and equations that define as best as possible the reality is a great step to know well how these beds behave, where the concept of randomness is so aggravating.

To close the study and see if it is necessary to perform a troubleshooting, the results are studied at a vector/contour picture level, in this way the behavior of the bed can be evaluated in a more dynamic and visual way. Also, to see if there are other parameters or variables in the model that bring the simulation to an unwanted point. In this way a crosschecking can be performed to ensure the correct behavior of the study and finally validate that the model is finalized.

The following vector/contour pictures (Figure 15, Figure 16, Figure 17, Figure 18 and Figure 19) show the water volume fraction (bed voidage) and the bulk density, at different times for each tested velocity. The bulk density is shown for each individual solid A, C and D. The different transient times and the steady state of computation will be shown in the contour pictures as A, B, C, D, E and F, being these, 0 s, 1 s, 10 s, 20 s, 50 s and 120 s respectively.

Analyzing Figure 15 above, some concepts can be clarified. As the time progresses from A to F, reaching in F the steady state, the randomness of the collisions and fluctuations of the solids can be seen, as well as the generated turbulence. In the steady state a characteristic segregation is finally achieved, where the solids of smaller diameter are fluidized at higher heights than those with a larger diameter, generating the aforementioned stratification.

Also, as the speed increases in the experiments, the heights reached by the solid packs with respect to the total height of the crystallization column are greater, as can be seen in Figure 11, Figure 12 and Figure 13. By representing the water volume fraction (bed voidage), different solids groups occupying their own phasic volume can be seen.

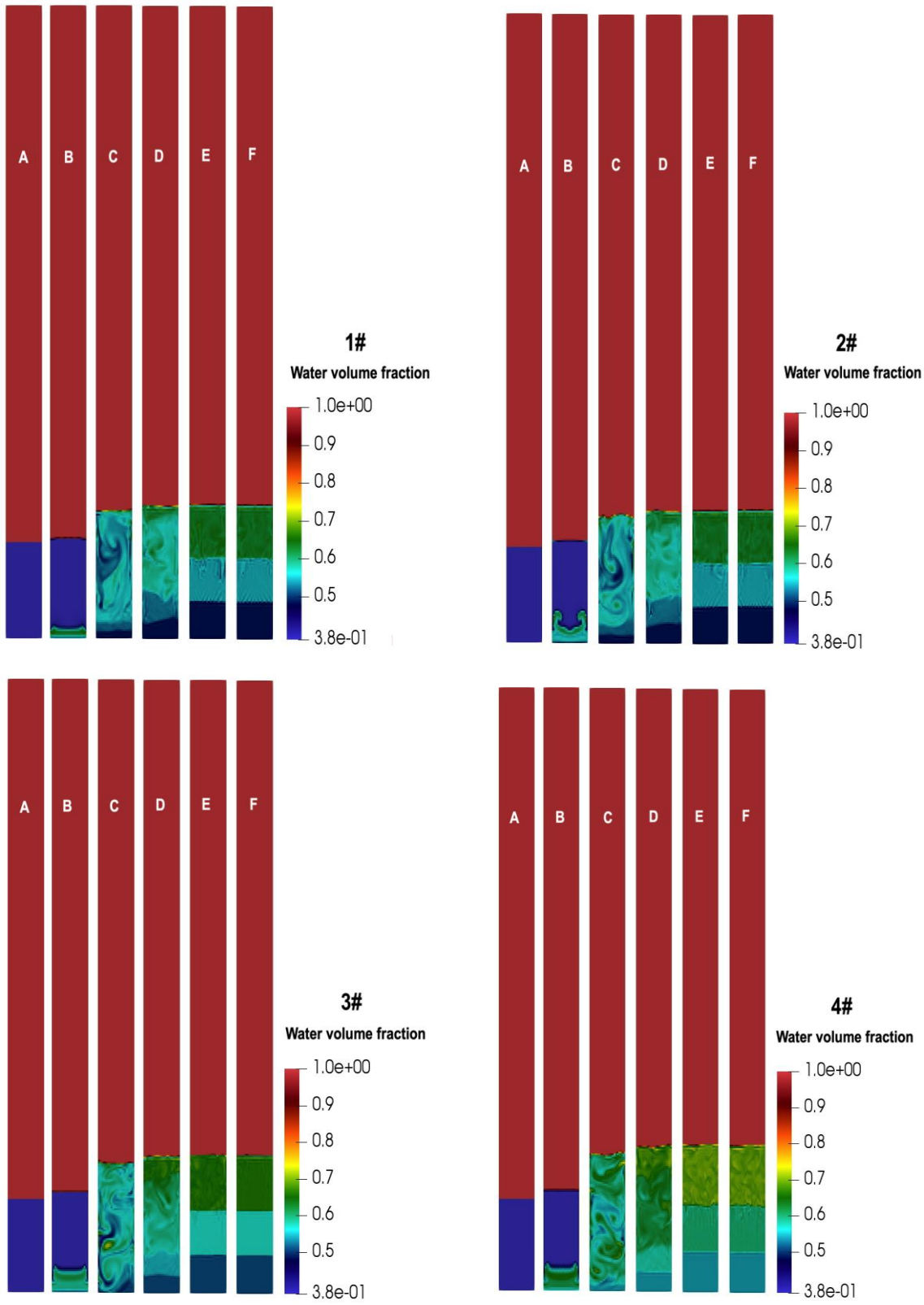

Figure 15. MFiX® & ParaView®. Water volume fraction (bed voidage). Experiments 1#, 2#, 3#, 4#.

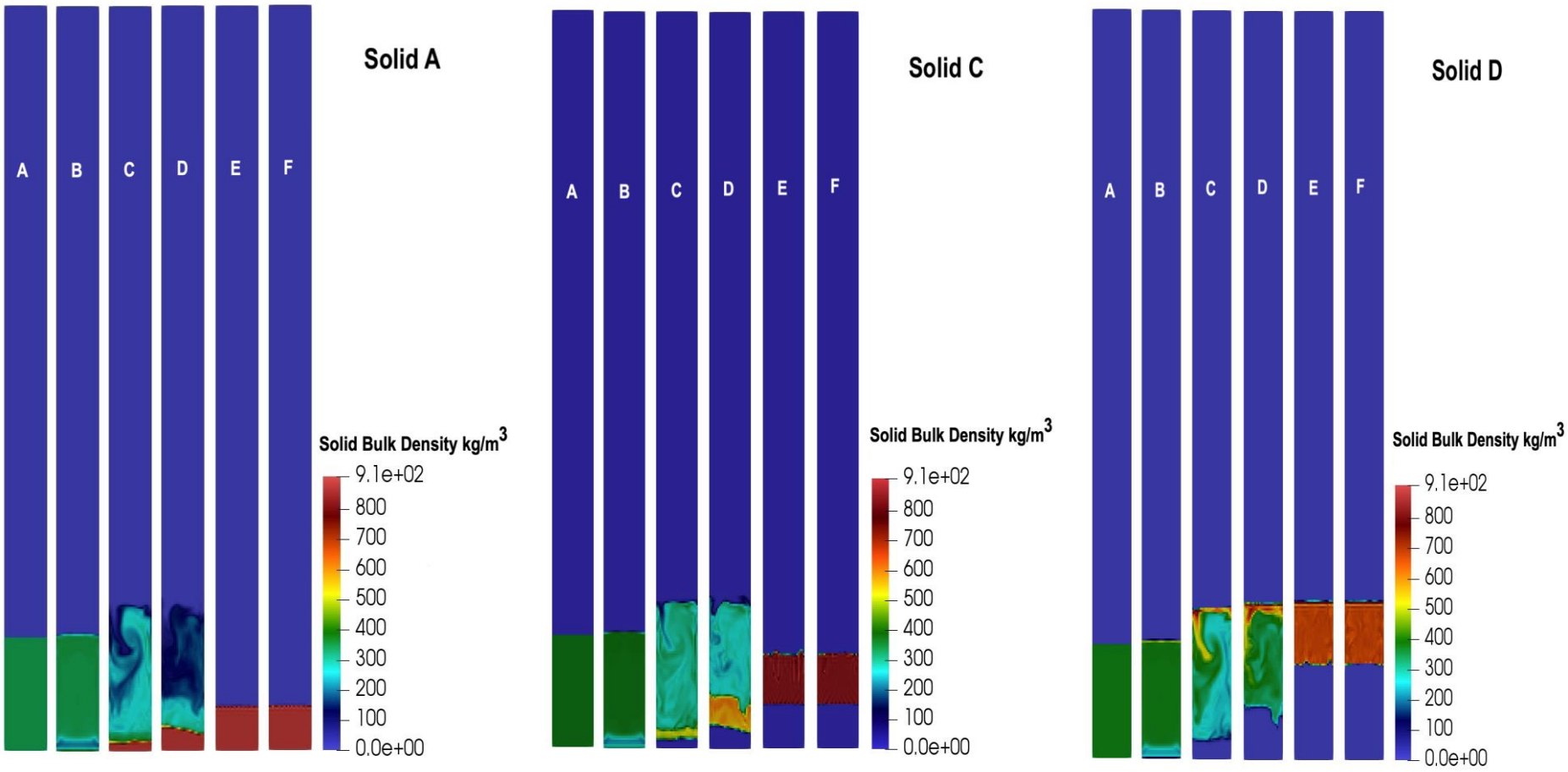

Figure 16. MFiX® & ParaView®. Solid bulk density. Experiment 1#.

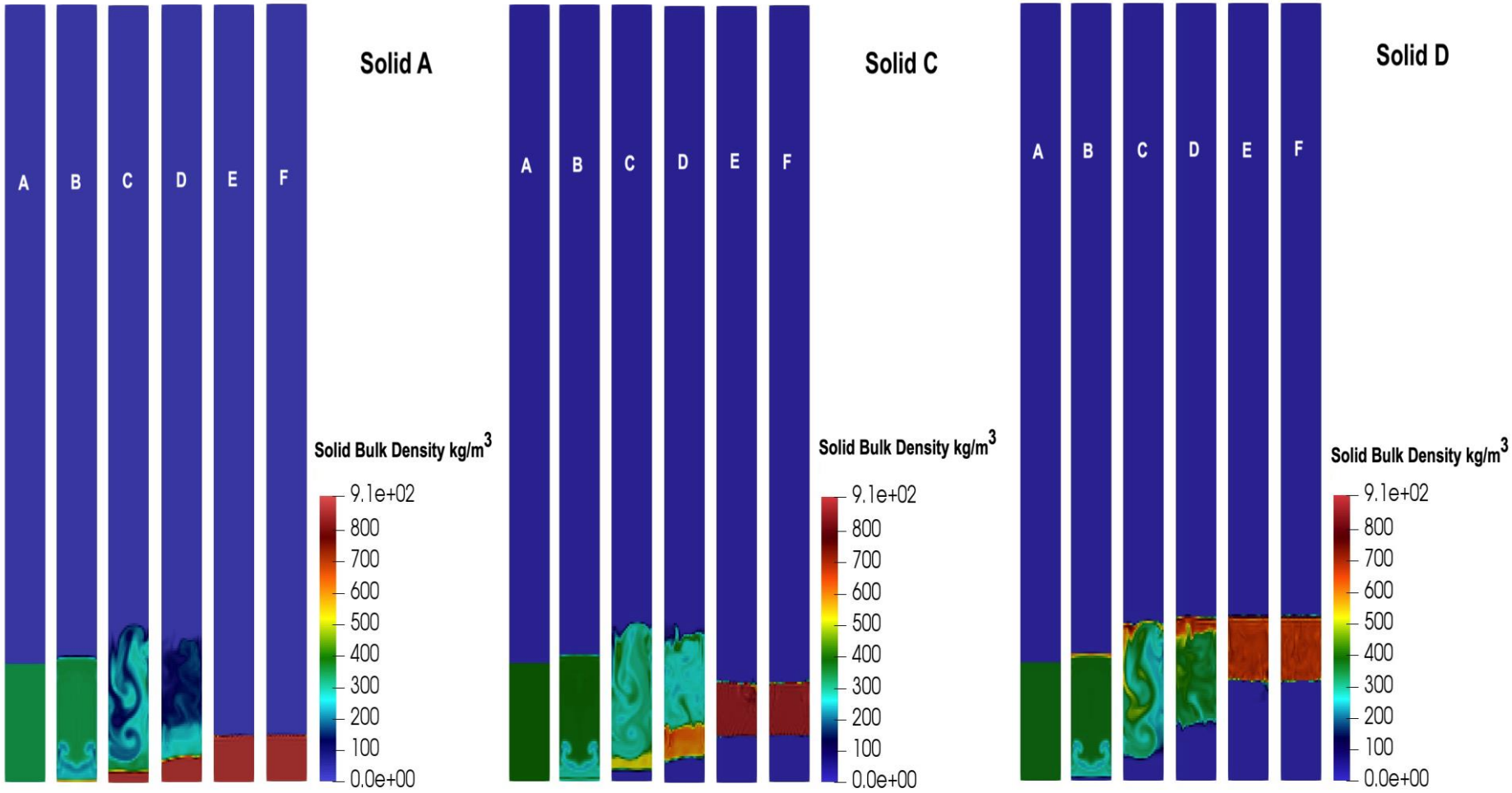

Figure 17. MFiX® & ParaView®. Solid bulk density. Experiment 2#.

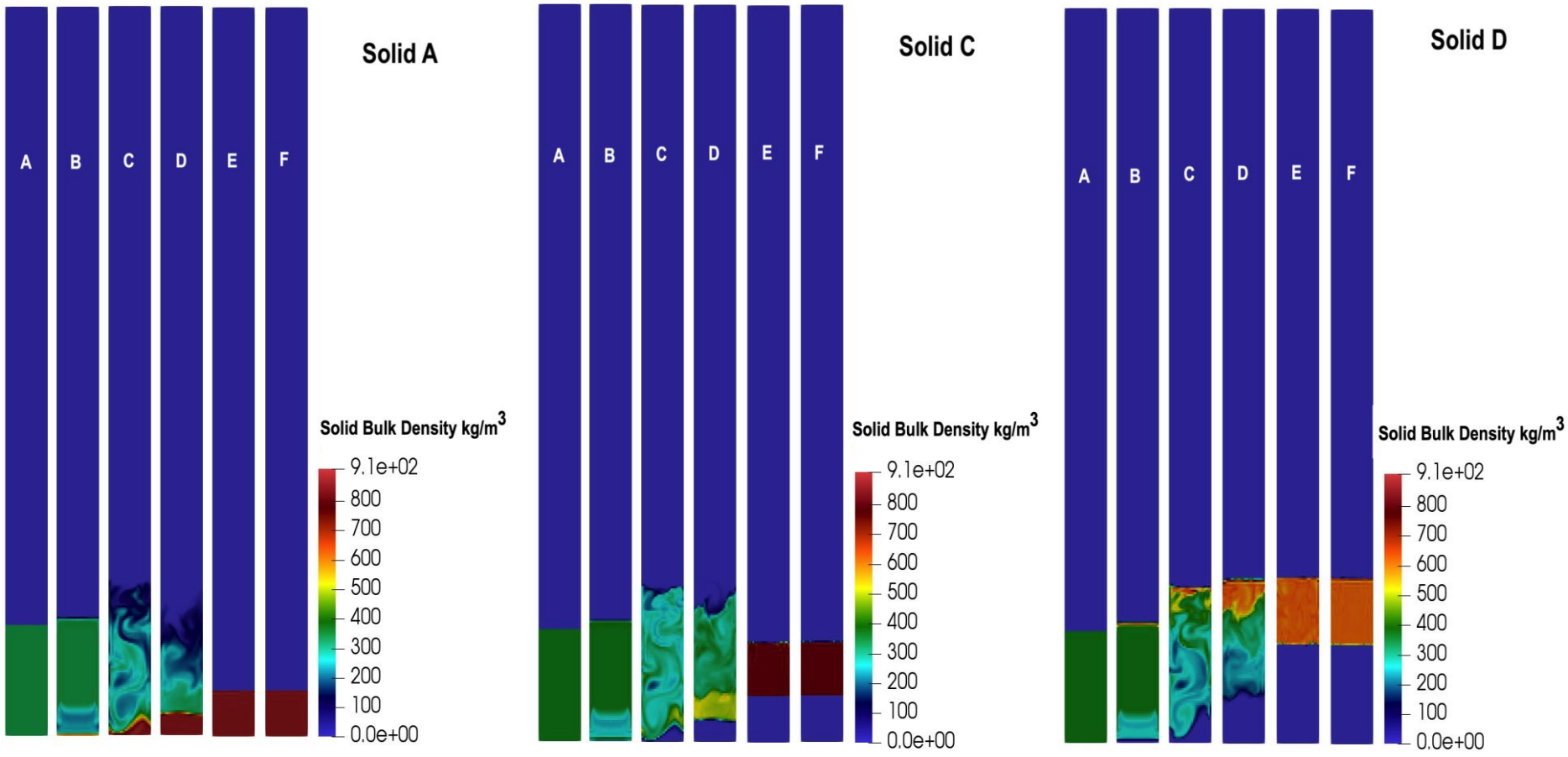

Figure 18. MFiX® & ParaView®. Solid bulk density. Experiment 3#.

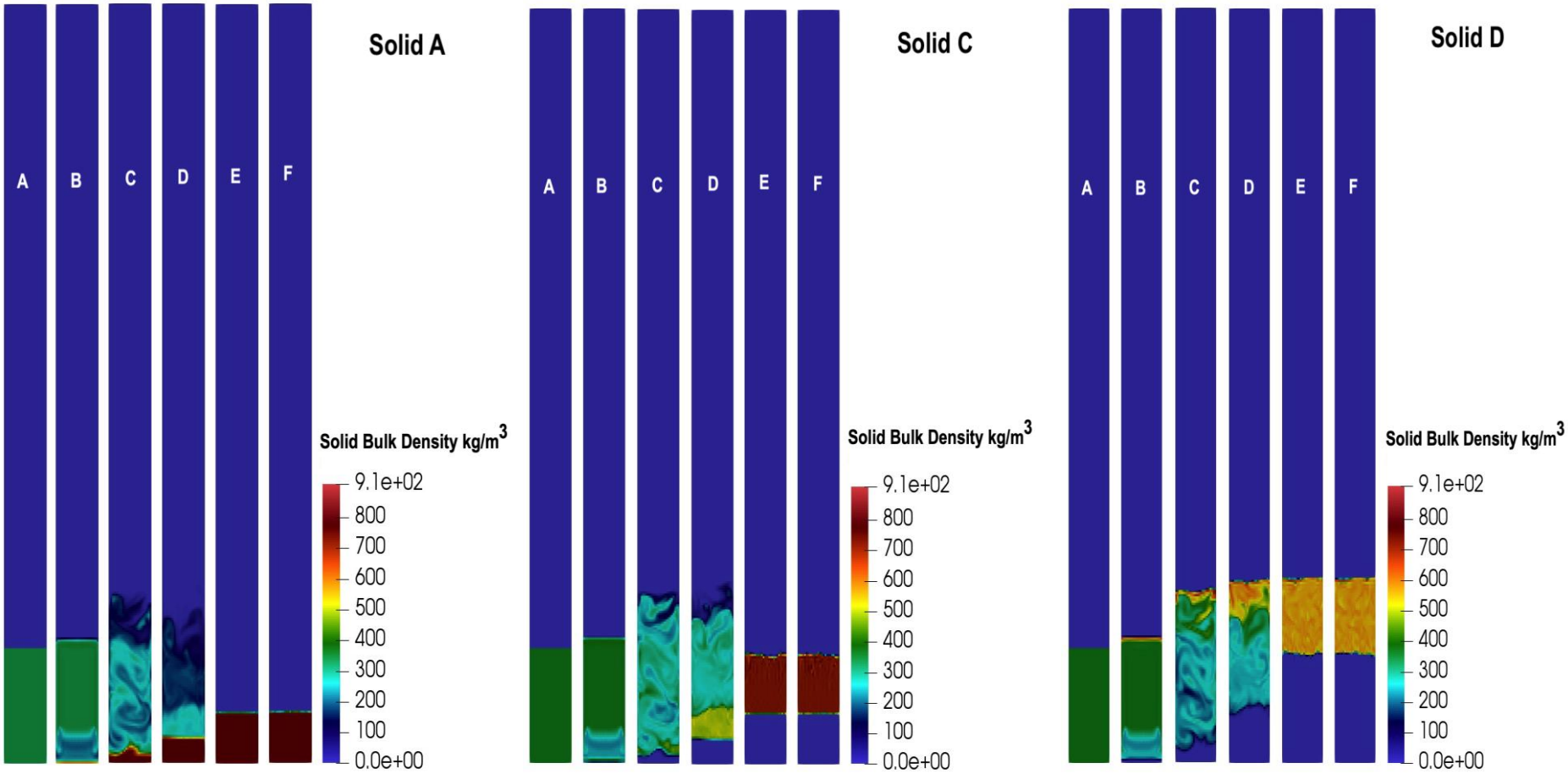

Figure 19. MFiX® & ParaView®. Solid bulk density. Experiment 4#.

As can be seen, in Figure 16, Figure 17, Figure 18 and Figure 19, that show the bulk density of each individual solid for each up-flow velocity there is a pattern. This pattern shows that in times E and F a steady state is achieved. From this, it can be concluded that the stationary time is reached much earlier than mentioned by (Md. Saifur, et al. 2017), at least at macroscopic level, more or less around the 50 s. At the graphical level (numerical level) and not at the vector/contour picture level, larger numerical variations can be observed, which implies microscopic variations in the behavior of the bed at a given time.

The steady state may exist at the theoretical level, but at the experimental (real) level it is not exactly a state where no magnitude varies. It is a state where everything varies little or at least where the variations of the magnitudes of the system fall within an interval or margin accepted as steady state.

In the case of computational fluid-dynamics (with dynamic studies, even if it sounds redundant), the models are prepared so that the system behaves as in reality. And sometimes waiting for a perfect steady state is not profitable because of temporary computing requirements. Many times, assessing trends and behavior of the system is enough. Therefore, often reaching a point of minimum variability between magnitudes is enough. This is what can be seen in Figure 16, Figure 17, Figure 18 and Figure 19, the difference between the time 50s and 120s is minimal. But if maximum accuracy is required, you have to go to the numerical level and wait until the real stationary state is reached.

Although, it can be observed that for each group of solids and each velocity study, the 3 groups of solids reach the steady state more or less at the same time. Therefore, the 3 solid groups reach their terminal velocity at the same time. It can also be observed how the solids of smaller diameter fulfill the previously explained premise, they do not generate a sudden segregation, but small noise zones (transient mixture areas) remain in the interface areas. That is due they can absorb more fluctuating kinetic/momentum energy from the fluid and collisions. Thereby they will never reach a true steady state, because they will never reach their terminal velocity.

If all the solids A, C and D are evaluated, in Figure 16, Figure 17, Figure 18 and Figure 19, it can be observed that in time C (10 s), the fluid begins to pass more forcefully through the layer of solids initially packaged and begins to ascend, causing fluidization. A very characteristic and known effect of transient states, where a fluid collides with a static solid, can be seen. This is known as the Von Kármán vortex street effect. In fluid dynamics, a Kármán vortex street (or a Von Kármán vortex street) is a repeating pattern of swirling vortices, caused by a process known as vortex shedding, which is responsible for the unsteady separation of flow of a fluid around blunt bodies. If the figures are evaluated correctly, it can be seen how the Von Karman Street swirl is produced by the fluid when it comes in contact with the larger solids that are located in the lower portion. It can also be observed that since the solids are not anchored and can be subject to fluidization, the phenomenon disappears once they got fluidized through the bed and the fluid stops seeing them as a wall, approximately at the time D (20s).

The Von Kármán vortex street effect can be evaluated more correctly in experiments 1# and 2#, Figure 16 and Figure 17, since the speed of the fluid is smaller and it does not have enough energy to transmit to the solids and fluidize them as fast as in experiments 3# and 4#, Figure 18 and Figure 19. The following Figure 21 shows a characteristic Von Kármán vortex street swirl. Take into account that in this figure the swirling effect is perfect, given that the solids against which the fluid collides are anchored and therefore

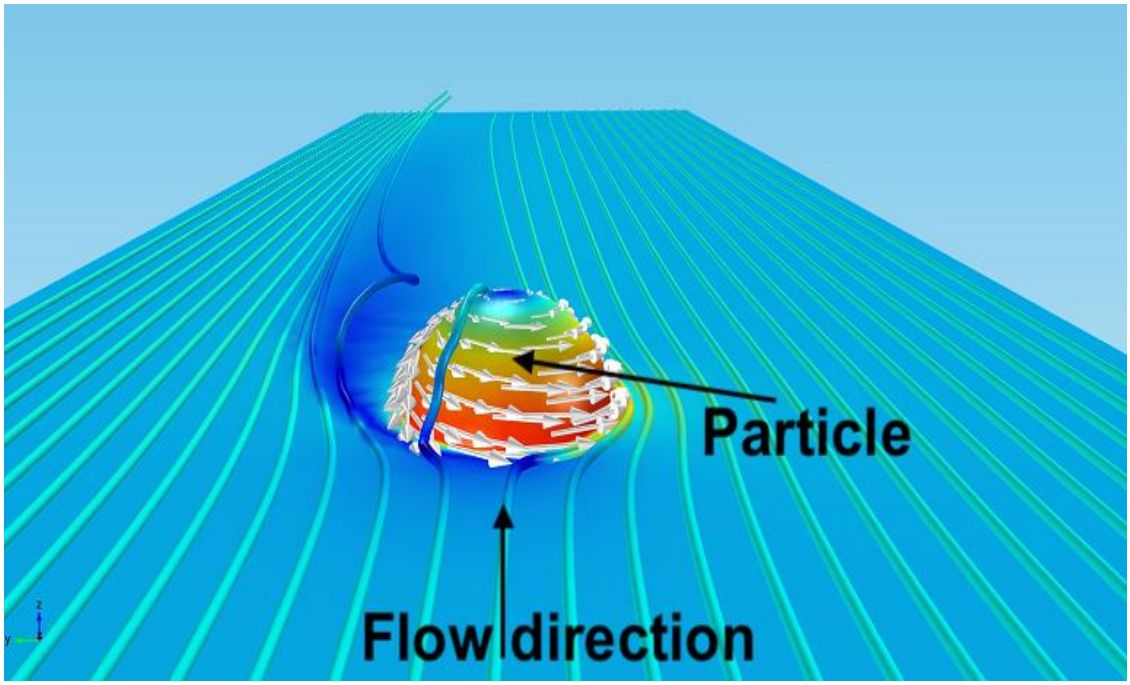

Figure 20. Flow over a particle. 3D render.

cannot be fluidized. This allows the system to generate perfect swirls. Therefore, the visual effect is not exactly the same as the effect of the previous figures, but to achieve the idea is enough. The image shown is taken in a totally random time. Note that a steady state with a fluid-solid contact configuration like this will never be reached.

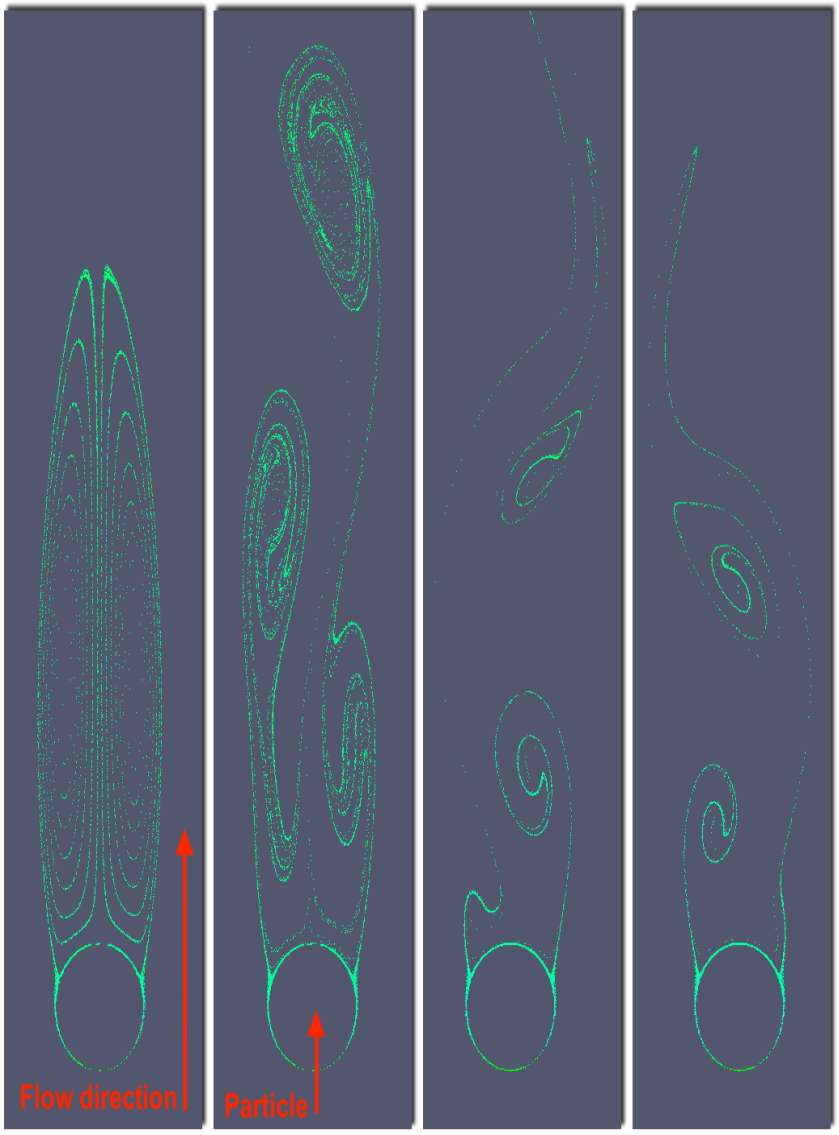

Figure 21. Von Kármán vortex street. Flow over a particle. (Coolfluid-3 2011-2015)

Figure 20 shows a solid not anchored. It is only shown to understand visually how a fluid collides with a solid. In this way it is easier to understand how the diameter of a particle can affect the transient and stationary states discussed so far. In summary, the greater the particle, the greater the Von Kármán vortex street effect (at least at visual

level). Also, as larger is the particle size, higher is the mass and more energy is required for the fluidization of the solid (higher fluid velocity provides greater kinetic energy that will be transmitted to the solid in contact with it), as shown in the previous results, where solid A (the bigger one) is fluidized in the bottom of the column due its high mass.

Something not mentioned above and therefore no less important, no preferential channels are observed. Therefore, it is understood that the solids can reach a state of correct and homogeneous mixture in all its final segregation pack volume and not only in the central axis of the crystallizer, as shown in the graphs studied previously where the data was plotted. Previously it has not been possible to explain this since the numerical results are delivered in a normalized vector format that goes from the base of the crystallization column to the upper portion of it, always passing through the central axis of the crystallizer. That is why it is very important in computational dynamic fluid studies to study the results at numerical level and also at vector or contours level.

7. CONCLUSIONS

A Eulerian-Eulerian Granular Two Fluid CFD model has been employed successfully to study the bed expansion characteristics of a fluidized bed of polydisperse struvite crystals in liquid media. Results of MFiX® simulations show the same pattern of bibliographic ANSYS® simulations and experimental data (Md. Saifur, et al. 2017); that is an increase in overall bed height and individual segregated particle size group heights with increasing superficial liquid velocity.

No preferential channels are observed in any study when reached the steady state, meaning that a homogeneous mixing is achieved for each solid segregated pack. Moreover, the CFD simulated, overall bed heights are found to be consistent with established correlations found in the literature (Md. Saifur, et al. 2017, Ergun 1993, Garside and Al-Dibouni. 1977) due that the constitutive relations for fluidized beds and the heuristic drag and meshing parameters are exported from this literature.

The mixing and segregation characteristics of this liquid and polydisperse struvite solid fluidized beds consisting of different sizes of struvite crystals captured by the CFD simulations are found to follow the basic principles of particle segregation (faster sedimentation and/or segregation at higher particle volumes and/or at lower fluid velocities).

At steady state, all three size groups of struvite are found to be classified according to their sizes, with limited intermixing noise (transient mixing areas) between successive layers of particle groups (interfaces).

Among the three empirical drag law correlations explained in this present study, when simulating the polydisperse struvite particle system and according to the expected predictions (Wen and Yu 1966, Gidaspow 1994) drag law models show a more accurate results to the experimental data than (Garside and Al-Dibouni. 1977) dump speed model, in terms of bed voidage.

8. CONTINUITY RECOMMENDATIONS

As goals to continue with fluidized bed simulations and to be able to study all the possible combinations of the system, the following proposals are included:

- Eulerian (static mesh) study of a fluidized bed column with at least three different solid types but same diameter.

- If enough computational capacity is available:
    - Eulerian (static mesh) study of a fluidized bed column with more than three different solid types but same diameter.
    - Eulerian (static mesh) study of a fluidized bed column with more than three different diameter types but same solid.
    - Lagrange (mobile mesh) studies of pipes with solids in suspension, these with different geometries that best aligns with the flow direction. The aim is to simulate solids as independent volumes. Not as in Eulerian models where all solids are equivalent spheres and only varies their diameter and density.

- Study only one fluidized Lagrange meshed solid:
    - Different fluid case studies (different fluid velocity)
    - Different solid case studies (different density)
    - Different solid case studies (different diameter)
    - Different solid shapes (to check solid-fluid-flow alignment & fluidization height reached for each shape for a same fluid flow velocity)

- Study any of the above cases with a fluid other than water:
    - With viscosity lower than that of water.
    - With viscosity higher than that of water.

9. REFERENCES

Adnan, A., Mavinic, D.S., Koch, F.A., 2003. Pilot-scale study of phosphorus recovery through struvite crystallization examining the process feasibility. J. Environ. Eng. Sci. 2 (5), 315–324.

Al-Rashed, M., Wojcik, J., Plewik, R., Synowiec, P., Kus, A., 2013. Multiphase CFD modeling: fluid dynamics aspects in scale-up of a fluidized-bed crystallizer. Chem. Eng. Process. 63, 7–15.

Bhuiyan, M.I.H., Mavinic, D.S., Beckie, R.D., 2008. Nucleation and growth kinetics of struvite in a fluidized bed reactor. J. Cryst. Growth 310 (6), 1187–1194.

Bhuiyan, M.I.H., Mavinic, D.S., Beckie, R.D., 2009. Dissolution kinetics of struvite pellets grown in a pilot-scale crystallizer. Can. J. Civil Eng. 36 (3), 550–558.

Booram, C.V., Smith, R.J., Hazen, T.E., 1975. Crystalline phosphate precipitation from anaerobic animal waste treatment lagoon liquors. Trans. Am. Soc. Agric. Eng. 18 (2), 340–343.

CED., 2019. Dewatering California Enviormental https://ced.biz/water-specialty-chemicals/struvite-removal/ 1/January.

Coolfluid 3 Scientific Software Framework, 2019. https://coolfluid.github.io. 9/April.

Lun, C.K.K., Savage, S.B., Jeffrey, D.J., Chepurniy, N., 1984. Kinetic theories for granular flow: inelastic particles in Couette flow and slightly inelastic particles in a general flow field. J. Fluid Mech. 140, 223–256.

Schaeffer, D.G., 1987. Instability in the evolution equations describing incompressible granular flow. J. Differ. Equ. 66 (1), 19–50.

Drew, D.A., 1983. Mathematical modeling of two-phase flow. Annu. Rev. Fluid Mech. 15 (1), 261–291.

Epstein, N., 2003. Liquid-solids fluidization. In: Yang, W.C. (Ed.), Handbook of Fluidization and Fluid-particle Systems. Marcel Dekker, New York, p. 91.

Ergun, S., 1952. Fluid flow through packed columns. Chem. Eng. Prog 4, 89–94. Felice, R.D., 1993. Mixing in Segregated, Binary-Solid Liquid-Fluidized Beds. Chem. Eng. Sci. 48 (5), 881–888.

Felice, R.D., 1995. Hydrodynamics of liquid fluidization. Chem. Eng. Sci. 50 (8), 1213–1245.

FLOW 3D., 2019. https://www.flow3d.com/resources/cfd-101/modeling-techniques/favor-vs-body-fitted-coordinates. 24/February.

Garside, J., Al-Dibouni, M., 1977. Velocity-voidage relationships for fluidization and sedimentation in solid-liquid systems. Ind. Eng. Chem. Process Des. Dev. 16 (2), 206–214.

Gibilaro, L.G., Felice, R.D., Waldram, S.P., Foscolo, P.U., 1985. Generalized friction factor and drag coefficient correlations for fluid-particle interactions. Chem. Eng. Sci. 40 (10), 1817–1823.

Gidaspow, D., 1994. Multiphase Flow and Fluidization: Continuum and Kinetic Theory Descriptions. Academic Press, Boston, MA, USA

Hoffman, R.F., Lapidus, L., Elgin, J.C., 1960. The mechanics of vertical moving fluidized systems: IV, Application to batch-fluidized systems with mixed particle sizes. AICHE J. 6, 321–324.

Lee, C.W., Kwon, H.B., Kim, Y.J., Jeon, H.P., 2005. Nutrients recovery by struvite formation from wastewater in a fluidized bed reactor. 6th International Symposium on Eco-Materials Processing & Design. Trans Tech Publications.

Mavinic, D.S., Koch, F.A., Huang, H., Lo, K.V., 2007. Phosphorus recovery from anaerobic digester supernatants using a pilot-scale struvite crystallization process. J. Environ. Eng. Sci. 6 (5), 561–571.

Md. Saifur Rahaman, Mahbuboor R. Choudhury, Amruthur S. Ramamurthy, Donald S. Mavinic, Naoko Ellis, Fariborz Taghipour, 2017. CFD modeling of liquid-solid fluidized beds of polydisperse struvite crystals. International Journal of Multiphase Flow 99 (2018), 48–61.

Paraview., 2018, https://www.paraview.org. 2/October

Syamlal, M., O'Brien, T.J., 1988. Simulation of granular layer inversion in liquid fluidized beds. Int. J. Multiphase Flow 14 (4), 473–481.

Syamlal, M., O'Brien, T.J., 2003. Fluid dynamic simulation of O3 decomposition in a bubbling fluidized bed. AICHE J. 49 (11), 2793–2801.

Versteeg., H.K., W. Malalasekera. 2007. Computational Fluid Dynamics, The Finite Volume Method, 2nd edition. Pearson, Prentice Hall.

Wen, C.Y., Yu, Y.H., 1966. Mechanics of fluidization. Chem. Eng. Prog. Symp. Ser. 62, 100–111.

Ye, X., Ye, Z.-L., Lou, Y., Pan, S., Wang, X., Wang, M.K., Chen, S., 2016a. A comprehensive understanding of saturation index and up-flow velocity in a pilot-scale fluidized bed reactor for struvite recovery from swine wastewater. Powder Tech- nol. 295, 16–26.

Ye, X., Chu, D., Lou, Y., Ye, Z.-L., Wang, M.K., Chen, S., 2016b. Numerical simulation of flow hydrodynamics of struvite pellets in a liquid-solid fluidized bed. J. Environ. Sci. doi: 10.1016/j.jes.2016.11.019, In Press.

Yoshino, M., Yao, M., Tsuno, H., Somiya, I., 2003. Removal and recovery of phosphate and ammonium as struvite from supernatant in anaerobic digestion. Water Sci. Technol. 48 (1), 171–178.

Zhang, H., Lo, V.K., Thompson, J.R., Koch, F.A., Liao, P.H., Lobanov, S., Mavinic, D.S., Atwater, J.W., 2015. Recovery of phosphorus from dairy manure: a pilot-scale study. Environ. Technol. 36 (11), 1398–1404.

10. NOMENCLATURE & SYMBOLS

Symbols

C_D	Drag coefficient
d_v	Equivalent diameter of particles.
e_{ss}	Restitution coefficient for particle collisions
F_l	External body force applied to liquid phase
F_{si}	External body force applied to the *ith* solid phase
g	Acceleration of gravity
$g_{o.ss}$	Radial distribution function of solids
$\hat{\mathrm{I}}$	Unit tensor
I_{2D}	Second invariant of the deviatoric stress tensor
k_c	Diffusion coefficient for solid phase energy fluctuation
$k_{l,s}$	Momentum exchange between solid-liquid phases
$k_{si,l} = k_{l,si}$	Momentum exchange coefficient between liquid and *ith* solid phases
$k_{sm,si}$	Momentum exchange coefficient between solid phases *m* and *i*
$Q_{l,si}$	Energy exchange between the liquid and the *ith* solid phases
P	Static pressure shared by all phases
P_s	Solid pressure
P_{si}	Solid pressure for *ith* solid phase
Re_s	Reynolds number

$u_{r,s}$	Terminal velocity correlation for the solid phase
v_l	Velocity vector for liquid phase
v_{si}	Velocity vector for *ith* solid phase
v_{sm}	Velocity vector for *mth* solid phase
Z	Stress tensor of different phases
Z_l	Stress tensors for the liquid phase
Z_{si}	Stress tensors for the *ith* solid phase

Greek letters

α_l	Volume fraction of liquid phase
α_s	Volume fraction of solid phase
α_{si}	Volume fraction of *ith* solid phase
$\alpha_{s,max}$	Maximum solid volume fraction in the bed
γ_{si}	Collisional dissipation of the energy
λ	Bulk viscosity of the phases
λ_s	Solid bulk viscosity
λ_l	Liquid bulk viscosity
μ	Shear viscosity of the phases
μ_l	Liquid shear viscosity
μ_s	Solid shear viscosity
$\mu_{s,col}$	Solid collisional shear viscosity

$\mu_{s,kin}$	Solid kinetic shear viscosity
$\mu_{s,frict}$	Solid frictional shear viscosity
ρ_l	Liquid density
ρ_{si}	*ith* solid density
θ	Angle of internal friction

Others

T_s	Granular temperature for solid phase
T_{si}	Granular temperature for *ith* solid phase
$\aleph_l$	Velocity tensor for liquid phase
$\aleph_{si}$	Velocity tensor for *ith* solid phase

Abbreviations

BNR	Biological nutrient removal
CFD	Computational fluid dynamics
FAVOR	Fractional area/volume method
MFP	Master final project
SAD	Secondary anaerobic digestion
2D	Two dimensions
3D	Three dimensions
EXP1 or 1#	Experiment 1, 18.26 mm/s boundary velocity inlet
EXP1 or 2#	Experiment 2, 22.70 mm/s boundary velocity inlet
EXP1 or 3#	Experiment 3, 25.29 mm/s boundary velocity inlet

EXP1 or 4#	Experiment 4, 28.68 mm/s boundary velocity inlet

11. APPENDIX

Table A.1. Errors between ANSYS® data and experimental data at selected heights.

EXP 1	Bed height (m)	Bed voidage	ERROR %
Experimental 1#	0.10	0.52	4.91
ANSYS®		0.49	
Experimental 1#	0.19	0.56	3.34
ANSYS®		0.58	
Experimental 1#	0.25	0.60	2.04
ANSYS®		0.59	

Table A.2. Errors between MFiX® data and experimental data at the experimental measurement heights.

EXP 1	Bed height (m)	Bed voidage	ERROR %
Experimental 1#	0.10	0.52	1.92
MFiX®		0.51	
Experimental 1#	0.19	0.56	1.79
MFiX®		0.57	
Experimental 1#	0.25	0.60	1.25
MFiX®		0.59	

Table A.3. Errors between ANSYS® data and experimental data at the experimental measurement heights.

EXP 2	Bed height (m)	Bed voidage	ERROR %
Experimental 2#	0.10	0.55	1.77
ANSYS®		0.54	
Experimental 2#	0.19	0.57	3.67
ANSYS®		0.59	
Experimental 2#	0.25	0.61	3.15
ANSYS®		0.63	

Table A.4. Errors between MFiX® data and experimental data at the experimental measurement heights.

EXP 2	Bed height (m)	Bed voidage	ERROR %
Experimental 2#	0.10	0.55	1.82
MFiX®		0.54	
Experimental 2#	0.19	0.57	1.75
MFiX®		0.58	
Experimental 2#	0.25	0.61	3.76
MFiX®		0.63	

Table A.5. Errors between ANSYS® data and experimental data at the experimental measurement heights.

EXP 3	Bed height (m)	Bed voidage	ERROR %
Experimental 3#	0.10	0.54	4.41
ANSYS®		0.56	
Experimental 3#	0.19	0.62	6.09
ANSYS®		0.66	
Experimental 3#	0.25	0.66	0.93
ANSYS®		0.65	

Table A.6. Errors between MFiX® data and experimental data at the experimental measurement heights.

EXP 3	Bed height (m)	Bed voidage	ERROR %
Experimental 3#	0.10	0.54	3.70
MFiX®		0.56	
Experimental 3#	0.19	0.62	3.23
MFiX®		0.64	
Experimental 3#	0.25	0.66	0.01
MFiX®		0.66	

Table A.7. Errors between ANSYS® data and experimental data at the experimental measurement heights.

EXP 4	Bed height (m)	Bed voidage	ERROR %
Experimental 4#	0.10	0.58	2.91
ANSYS®		0.60	
Experimental 4#	0.19	0.62	4.15
ANSYS®		0.59	
Experimental 4#	0.25	0.69	0.72
ANSYS®		0.69	

Table A.8. Errors between MFiX® data and experimental data at the experimental measurement heights.

EXP 4	Bed height (m)	Bed voidage	ERROR %
Experimental 4#	0.10	0.58	3.73
MFiX®		0.60	
Experimental 4#	0.19	0.62	3.23
MFiX®		0.60	
Experimental 4#	0.25	0.69	0.88
MFiX®		0.68	